THESIS

THE AUTISM-ASSOCIATED LOSS OF δ-CATENIN FUNCTION DISRUPTS SOCIAL BEHAVIOR AND PREFRONTAL NETWORK ACTIVITY

Submitted by

Regan Lynn Roach

Department of Biomedical Sciences

In partial fulfillment of the requirements

For the Degree of Master of Science

Colorado State University

Fort Collins, Colorado

Summer 2025

Master's Committee:

Advisor: Seonil Kim

Michael Tamkun
Susan Tsunoda
Julie Moreno

ABSTRACT

THE AUTISM-ASSOCIATED LOSS OF δ-CATENIN FUNCTION DISRUPTS SOCIAL BEHAVIOR AND PREFRONTAL NETWORK ACTIVITY

Social behavior is imperative for survival in humans and many other species. There are various neurological disorders that indicate social impairment as a primary symptom. Previous works have suggested that synaptic structure and subsequent function can regulate social behavior, although the link between these is not yet fully understood. δ-catenin is expressed in excitatory synapses and functions as an anchor for the glutamatergic AMPA receptor (AMPAR) GluA2 subunit in the postsynaptic density. The glycine 34 to serine (G34S) mutation in the *δ-catenin* gene has been found in autism spectrum disorder (ASD) patients and results in a loss of δ-catenin functions at excitatory synapses, which is presumed to underlie ASD pathogenesis in humans. Our previous study using neuroblastoma cells has identified that the G34S mutation increases glycogen synthase kinase 3β (GSK3β)-dependent δ-catenin degradation to reduce δ-catenin levels, which likely contributes to the loss of δ-catenin functions. However, how the G34S mutation causes a loss of δ-catenin functions to induce synaptic dysfunction related to ASD-associated behaviors remains unclear, as does the effect of an overall loss of δ-catenin. My thesis work with colleagues reveals that synaptic δ-catenin and GluA2 levels in the cortex are significantly decreased in mice harboring the δ-catenin G34S mutation and the δ-catenin knockout (KO). In addition, the δ-catenin G34S and KO increase glutamatergic activity in cortical excitatory neurons while they decrease in inhibitory interneurons, indicating changes in cellular excitation and inhibition. This is important for brain network activity that contributes to multiple behaviors including social interaction. We in fact show that δ-catenin G34S and KO

mutant mice exhibit social dysfunction, a common feature of ASD. Additionally, δ-catenin G34S mutant mice display altered network activity within the medial prefrontal cortex (mPFC), which likely underlies social deficit. In fact, abnormalities in prefrontal network activity has been reported in several studies of ASD. Most importantly, pharmacological inhibition of GSK3β activity reverses the G34S-induced loss of δ-catenin function effects in cells and mice. Finally, using δ-catenin KO mice, we confirm that δ-catenin is required for GSK3β inhibition-induced restoration of normal social behavior and prefrontal network activity in δ-catenin G34S mutant animals. Taken together, my work reveals that the loss of δ-catenin functions arising from the ASD-associated G34S mutation and δ-catenin KO mutation induce social dysfunction via alterations in activity at the synaptic, cellular, and network levels and that GSK3β inhibition can reverse δ-catenin G34S-induced synaptic and behavioral deficits.

ACKNOWLEDGEMENTS

I would like to thank the members of the Kim Laboratory at Colorado State University for their support. In particular, I would like to thank my predecessors who greatly contributed to this project and generated the foundational data, including Kaila Nip, Matheus Sathler, and Hadassah Mendez-Vazquez. I would also like to acknowledge and thank my committee members, Dr. Michael Tamkun, Dr. Susan Tsunoda, and Dr. Julie Moreno for their support and guidance through the duration of my project and degree program. I am grateful to my fellow graduate students in the Kim lab and the time we spent together, forming strong bonds as both colleagues and friends. I would also like to thank my family for their support and encouragement that they have generously given throughout the course of this degree program.

Lastly, I would like to thank Dr. Seonil Kim for being my advisor. In the past few years, I have been able to exponentially grow my confidence in both my academic and technical abilities, which would not have been possible without the guidance of Dr. Kim. I will always appreciate the time I have spent in the Kim lab, the friends I have made, and the research I have done.

TABLE OF CONTENTS

LIST OF FIGURES

INTRODUCTION[1]

Social behavior is essential for the survival of many species [1]. However, our knowledge of the physiological, cellular, and molecular mechanisms driving social behavior is still limited [1]. Various mental disorders, including autism spectrum disorder (ASD), anxiety, depression, and schizophrenia, have social impairment as a primary symptom [2-5]. In particular, autism spectrum disorder is a neurodevelopmental disorder characterized by its effect on an individual's ability to interact and communicate with others, with common symptoms including repetitive behaviors and restricted interests [6]. There are several underlying causes of autism, but we do not yet know the cause on a case-by-case basis. There are some environmental factors, such as exposure to valproic acid in utero [7], that have been shown to cause ASD, however it is generally believed that genetics heavily influence an individual's risk of ASD [6]. Furthermore, the prevalence of individuals diagnosed with ASD has increased throughout the past several years, with approximately 1 in 31 children having diagnosed ASD in the surveillance year of 2022, whereas the prevalence observed in the surveillance year of 2012, just ten years prior, was 1 in 69 children [8]. The increase in ASD prevalence observed in recent years is indicative of improved screenings and greater awareness for the neurodevelopmental disorder [9]. It is also important to consider the possibility of sex differences in the underlying mechanisms of social behavior, as the prevalence of ASD is approximately 3.4 times greater in males than in females, of which could be due to previous research on ASD using primarily male subjects or assessing male phenotypes for the disorder [10]. It is possible that the phenotypic expression of ASD as well as the underlying mechanisms or activity levels in the brain could differ between male and female patients, but this is not yet fully understood. Therefore,

[1] Mendez-Vazquez, H., Roach, R. L., Nip, K., Chanda, S., Sathler, M. F., Garver, T., Danzman, R. A., Moseley, M. C., Roberts, J. P., Koch, O. N., Steger, A. A., Lee, R., Arikkath, J., Kim, S., *The autism-associated loss of delta-catenin functions disrupts social behavior.* Proc Natl Acad Sci U S A, 2023. 120(22): p. e2300773120.

improving knowledge of the mechanisms mediating social behavior can help us to better understand these diseases and develop effective treatments.

Given that the mechanisms underlying disorders such as ASD which pertain to social behavior are not yet entirely understood, treatments for such disorders typically do not focus on their potential genetic basis, but rather on therapeutic models that can be implemented with the use of Applied Behavior Analysis (ABA) and Social Skills Training (SST), which focus on skill improvement of affected individuals by means of behavioral, educational, and psychological therapies to encourage or discourage desired and undesired behaviors, respectively [9]. There are some pharmaceutical treatments for ASD that are currently used, however these primarily focus on symptoms of ASD that pertaining to the irritability associated with disorder [11], a symptom that does not necessarily occur in all individuals with ASD [6]. While treatments that focus on intervention and symptom improvement can have high efficacy rates [9], a greater understanding of the foundational causes for disorders that cause deficits in social behavior will allow us to develop further treatments that can be used in parallel with current treatment methods to potentially yield even greater results.

A large body of studies illustrates the idea that varied synaptic activity and signaling contribute to the initiation, maintenance, and/or modulation of social behavior [1]. However, the relationship between synaptic regulation and social behavior is not completely understood. Postsynaptic glutamatergic activity in excitatory and inhibitory cells in multiple brain regions is crucial for social behavior [12-18]. In addition, abnormalities in prefrontal oscillations have been implicated in several studies of ASD [12, 17, 19]. Disruptions in excitatory connectivity have been implicated in individuals with ASD and in mouse models of ASD [19-27]. This disruption in activity can be observed through neural oscillations in the prefrontal region of the brain [6]. Theta and gamma oscillations have a functional role in neuronal communication regarding memory encoding/retrieval and data processing, all of which are essential for social behavior

[28, 29]. However, it is not well understood how postsynaptic glutamatergic activity and/or network level activity regulate social behavior.

Several human genetic studies suggest that the *δ-catenin* gene is strongly linked to ASD [27, 30-34]. Notably, genetic alterations in the *δ-catenin* gene are associated with severely affected ASD patients from multiple families [30, 32, 33]. δ-catenin is a member of the armadillo repeat protein family that is highly expressed in neurons and localizes to the excitatory and inhibitory synapses [34-40]. At the postsynaptic density (PSD) in the excitatory synapse, δ-catenin interacts with the intracellular domain of N-cadherin, a synaptic cell adhesion protein, and the carboxyl terminus of δ-catenin binds to AMPA-type glutamate receptor (AMPAR)-binding protein (ABP) and glutamate receptor-interacting protein (GRIP) (**Figure 1**) [34, 37-39, 41, 42]. This N-cadherin-δ-catenin-ABP/GRIP complex functions as an anchor for the AMPAR GluA2 subunit (**Figure 1**). This complex is disrupted when δ-catenin functions are lost [34, 39, 43, 44]. Importantly, some δ-catenin ASD mutations are unable to reverse the δ-catenin deficiency-induced loss of excitatory synapses in cultured mouse neurons, suggesting that these mutations cause a loss of δ-catenin functions [33]. Moreover, δ-catenin expression is closely linked to other ASD-risk genes involved in synaptic structure and function, such as GluA2, cadherins, GRIP and synaptic Ras GTPase activating protein 1 (SYNGAP1), further illustrating its importance for synaptic pathophysiology and social dysfunction in ASD [40, 45-47]. This indicates that δ-catenin deficiency induces ASD-associated social deficits via impairment of glutamatergic synapses.

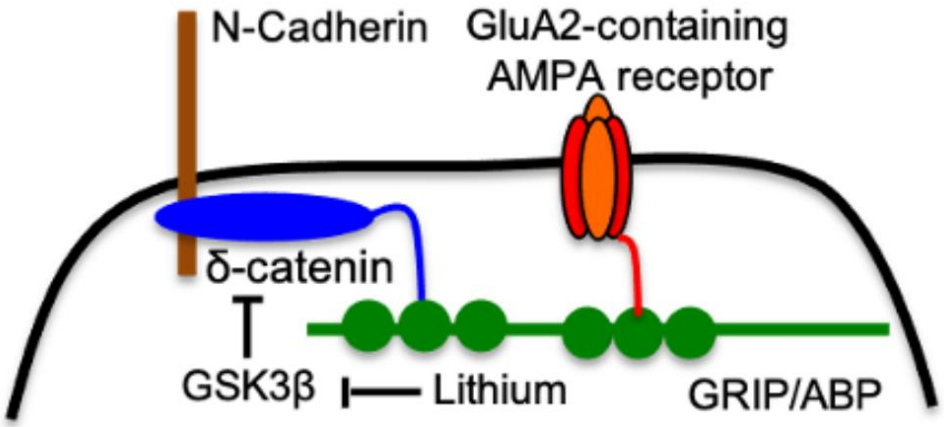

Figure 1. A schematic of N-cadherin-δ-catenin-ABP/GRIP-GluA2 synaptic complex.

A schematic of N-cadherin-δ-catenin-ABP/GRIP-GluA2 synaptic complex and GSK3b regulation of δ-catenin. At PSD, δ-catenin interacts with N-cadherin, a synaptic cell adhesion protein. The carboxyl-terminus of δcatenin binds to AMPA receptor-binding protein (ABP) and glutamate receptor-interacting protein (GRIP). This N-cadherin-δ-catenin-ABP/GRIP complex functions as an anchor for GluA2. GSK3β phosphorylates δ-catenin, which leads to δ-catenin degradation. The reduction of GSK3β activity by lithium stabilizes the N-cadherin-δcatenin-ABP/GRIP-GluA2 complex.

Overall, the molecular and cellular links between δ-catenin functions, synaptic activity, and social behavior are largely unknown. Among the ASD-associated δ-catenin missense mutations, the glycine 34 to serine (G34S) mutation exhibits a profound loss of δ-catenin functions in excitatory synapses (**Figure 3**). It has been previously shown that glycogen synthase kinase 3 beta (GSK3β) phosphorylates threonine 1078 (T1078) of δ-catenin, leading to δ-catenin ubiquitination and subsequent proteasome-mediated degradation, whereas inhibition of GSK3β elevates δ-catenin levels (**Figure 2**) [38, 48, 49]. The Group-based Prediction System [50] predicts that the G34S mutation in the amino-terminus of δ-catenin mimics one of the β-catenin phosphorylation sites (**Figure 2**), which may provide an extra site for GSK3β-mediated phosphorylation of δ-catenin in addition to T1078 (**Figure 2**). This could accelerate the degradation of δ-catenin, causing it to lose its function. In fact, our previous work reveals that the δ-catenin G34S mutation reduces δ-catenin levels, which is mediated by proteasomal degradation [51]. To further investigate whether reduced expression of δ-catenin is dependent on GSK3β and is the primary cause of reduced δ-catenin in the G34S mutation, the

previous study employed pharmacological and genetic techniques to inhibit GSK3β [51]. They found that inhibition of GSK3β using lithium chloride (LiCl) led to a marked increase in both WT and G34S δ-catenin levels, coinciding with elevated phosphorylation at serine 9 of GSK3β indicative of its inactivation [51]. Additionally, they found that knockdown of GSK3β siRNA effectively reduced GSK3β levels and restored G34S δ-catenin levels comparable to those found in WT cells, supporting the idea of GSK3β having a regulatory role in δ-catenin expression [51]. Altogether, this suggests the G34S mutation accelerates GSK3β-mediated δ-catenin degradation, leading to δ-catenin function loss, of which can be restored with the use of lithium treatment [51].

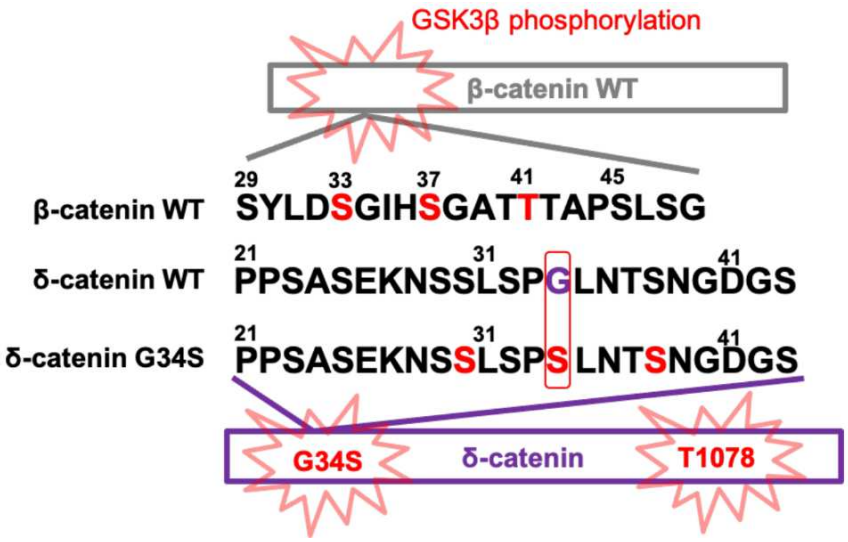

Figure 2. Amino acid sequence homology between β-catenin, WT δ-catenin and G34S WT δ-catenin.

The δ-catenin G34S mutation adds an additional GSK3β-mediated phosphorylation site to induce δ-catenin degradation. GSK3β phosphorylation sites of b-catenin in the amino-terminal region known to induce proteasomal degradation of β-catenin highlighted in red (S33, S37, and T41) are comparable to possible GSK3β phosphorylation sites in the amino-terminus of G34S mutant δ-catenin also highlighted in red (S30, S34, and S38). In addition to GSK3β-mediated threonine 1078 phosphorylation site in the carboxyl-terminus of δ-catenin, these potential amino-terminal GSK3β-mediated phosphorylation sites may enhance δ-catenin degradation.

Although the previous work has shown the cellular mechanism underlying the δ-catenin G34S mutation-induce loss of function, how the δ-catenin G34S mutation induces social deficits in ASD is not understood. To better understand this mutation, our lab employed a δ-catenin

G34S knockin mouse line generated by Dr. Jyothi Arikkath at University of Nebraska Medical Center (UNMC) Mouse Genome Engineering Core utilizing the CRISPR-Cas9 technique [51]. The previous work found a significant reduction in synaptic δ-catenin and GluA2 levels in the female and male G34S animals' cortices when compared to the WT cortex, but no difference in synaptic GluA1 levels between the WT and G34S cortex In the PSD fraction (**Figure 3**) [51]. They further examined if lithium-based pharmacological inhibition of in vivo GSK3β activity reversed the δ-catenin G34S mutation's effects on synaptic δ-catenin and AMPAR levels in the cortex, of which was carried out in my research as well. They found via immunoblotting that the levels of both δ-catenin and GluA2 in the cortex of male and female G34S mutant mice were restored to the levels observed in the male and female WT cortices (**Figure 3**) [51] .

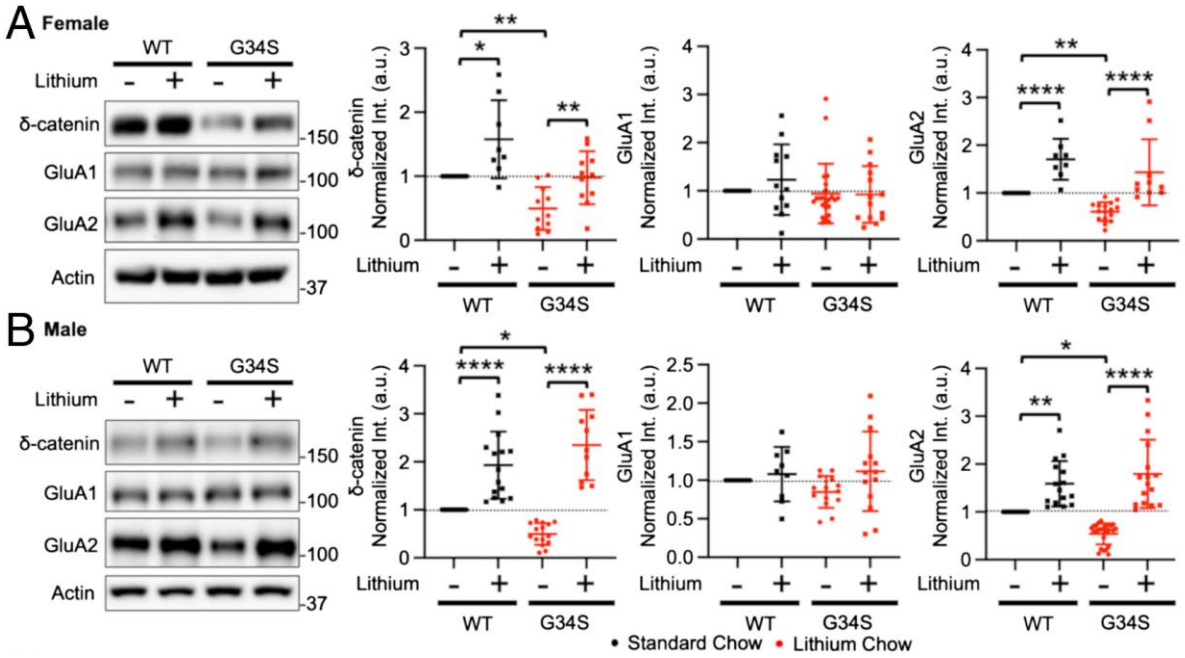

Figure 3. Lithium treatment reverses a significant reduction of synaptic δ-catenin and GluA2 in the δ-catenin G34S cortex.

Representative immunoblots and summary graphs of normalized δ-catenin, GluA1, and GluA2 levels in the cortical PSD fractions from standard chow (−) or lithium chow (+)-fed WT and δ-catenin G34S **(A)** female (n = number of immunoblots [number of mice]. For δ-catenin, WT + standard chow =14 [5], WT + lithium chow = 8 [5], G34S + standard chow = 11 [6], and G34S + lithium chow = 11 [6]. For GluA1, WT + standard chow = 14 [5], WT + lithium chow = 12 [5], G34S + standard chow = 23 [6], and G34S + lithium chow = 14 [6]. For GluA2, WT + standard

chow = 11 [5], WT + lithium chow = 8 [5], G34S + standard chow = 16 [6], and G34S + lithium chow = 10 [6]) and **(B)** male mice (n = number of immunoblots [number of mice]. For δ-catenin, WT + standard chow = 17 [5], WT + lithium chow = 15 [5], G34S + standard chow = 15 [6], and G34S + lithium chow = 11 [6]. For GluA1, WT + standard chow = 14 [5], WT + lithium chow = 9 [5], G34S + standard chow = 14 [6], and G34S + lithium chow = 14 [6]. For GluA2, WT + standard chow = 18 [5], WT + lithium chow = 15 [5], G34S + standard chow = 24 [6], and G34S + lithium chow = 15 [6], *P < 0.05, **P < 0.01, and ****P < 0.0001, Two-way ANOVA with the Tukey test). The position of molecular mass markers (kDa) is shown on the right of the blots. Experiments performed by Hadassah Mendez-Vazquez.

To further examine both the impact of the G34S mutation itself and the impact of this inactivation of GSK3β activity on synaptic activity, glutamate uncaging was performed by a previous lab member on WT and G34S cortical neurons. With this, they found that while glutamatergic activity is significantly increased in G34S cortical excitatory neurons as compared to WT cortical excitatory neurons (**Figure 4A**), glutamatergic activity was significantly reduced in G34S inhibitory interneurons as compared to their WT counterparts (**Figure 4B**) [51]. Both changes observed in glutamatergic activity in the G34S cortical neurons were reversed with the transfection of lithium chloride (LiCl) (**Figure 4 A and B**) [51].

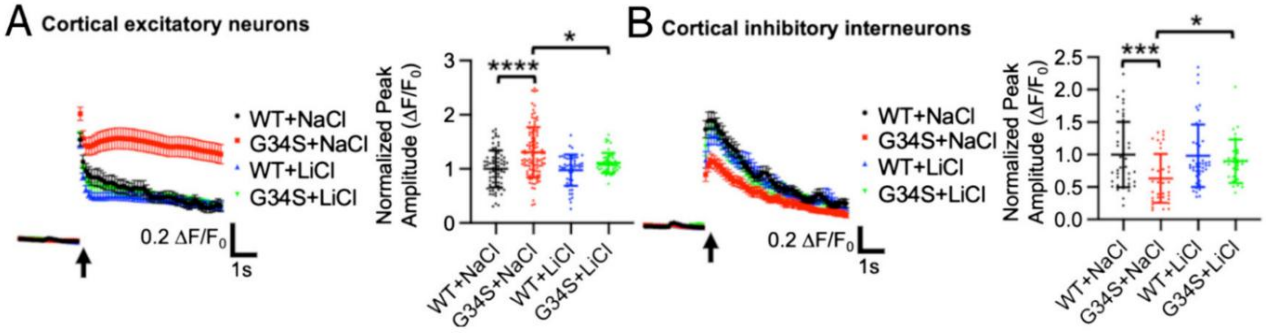

Figure 4. Altered glutamatergic activity in cultured G34S cortical neurons.

(A) Average traces of GCaMP7s signals and summary data of normalized peak amplitude in each condition in excitatory neurons (n = number of neurons from 3 independent cultures, WT = 70 and KO = 73). **(B)** Average traces of GCaMP6f signals and summary data of normalized peak amplitude in each condition in inhibitory interneurons (n = number of neurons from three independent cultures, WT = 38 and KO = 30, ***P < 0.01 and ****P < 0.0001, the unpaired two-tailed Student's t test). An arrow indicates photostimulation. Mean ± SD. Experiments performed by Hadassah Mendez-Vasquez.

Altogether, my colleagues have demonstrated that δ-catenin G34S significantly alters AMPAR-mediated glutamatergic activity in excitatory and inhibitory cells in opposite ways, which likely disrupts the neuronal E/I balance in the cortex. Moreover, we find that these changes in G34S mutant neurons are reversed by pharmacological inhibition of GSK3β. As previously mentioned, pharmaceutical therapies are a substantially less studied option for treatment of ASD [6, 9], whereby the examination of this form of treatment for the autism-associated loss of a synaptic protein such as δ-catenin is both nuanced and important for progression in the development of such treatments within the field.

RESULTS[1]

δ-Catenin G34S Induces Social Dysfunction in Mice, Which Is Reversed by GSK3β Inhibition.

A three-chamber test was performed to determine whether the δ-catenin G34S mutation affected social behavior [52]. We identified that WT female and male mice interacted significantly longer with stranger 1 than the novel object during the sociability test, an indication of normal sociability (**Figure 5**). Conversely, in δ-catenin G34S female and male mice, no significant difference in total interaction time was found between stranger 1 and the novel object (**Figure 5**). Importantly, social interaction time with stranger 1 in δ-catenin G34S female and male mice was significantly less than WT mice (**Figure 5**). In the social novelty test, WT mice engaged with stranger 2 for longer than they did with stranger 1, demonstrating normal social novelty preference (**Figure 6**). However, there was no significant difference in reciprocal sniffing time between stranger 1 and stranger 2 in δ-catenin G34S female and male mice (**Figure 6**). Crucially, compared to WT mice, social interaction with stranger 2 was markedly lower in both female and male δ-catenin G34S animals (**Figure 6**). These findings indicate that δ-catenin G34S mice exhibit disrupted sociability and social novelty preference in the three-chamber test. As lithium treatment significantly reduced GSK3β activity and elevated synaptic δ-catenin and GluA2 expression in the δ-catenin G34S cortex (**Figure 3**), we examined whether lithium treatment could restore normal social behavior in mutant mice using the three-chamber test. In the sociability test, we identified that both WT and δ-catenin G34S female and male mice fed with lithium chow interacted with stranger 1 for significantly longer than they did with the novel object, indicating that reduced GSK3β activity reversed disrupted sociability in δ-catenin G34S mice (**Figure 5**). Furthermore, we found that lithium treatment significantly increased social interaction time with stranger 1 in δ-catenin G34S mice in the sociability test compared to those before lithium (**Figure 5**). The discrimination index further confirmed that lithium treatment

reversed impaired sociability in δ-catenin G34S female and male mice (**Figure 5**). We also revealed that lithium-fed WT and δ-catenin G34S female and male mice interacted significantly longer with stranger 2 than stranger 1 during the social novelty test, showing that lithium treatment restored normal social novelty preference in δ-catenin G34S mice (**Figure 6**). In addition, social interaction with stranger 2 in δ-catenin G34S mice was significantly elevated following lithium treatment in the social novelty test compared to those before lithium (**Figure 6**). Finally, the discrimination index confirmed that lithium treatment restored normal social novelty preference behavior in δ-catenin G34S female and male mice (**Figure 6**). Taken all together, δ-catenin G34S disrupts social behavior in mice, which is reversed by lithium-based pharmacological inhibition of in vivo GSK3β activity.

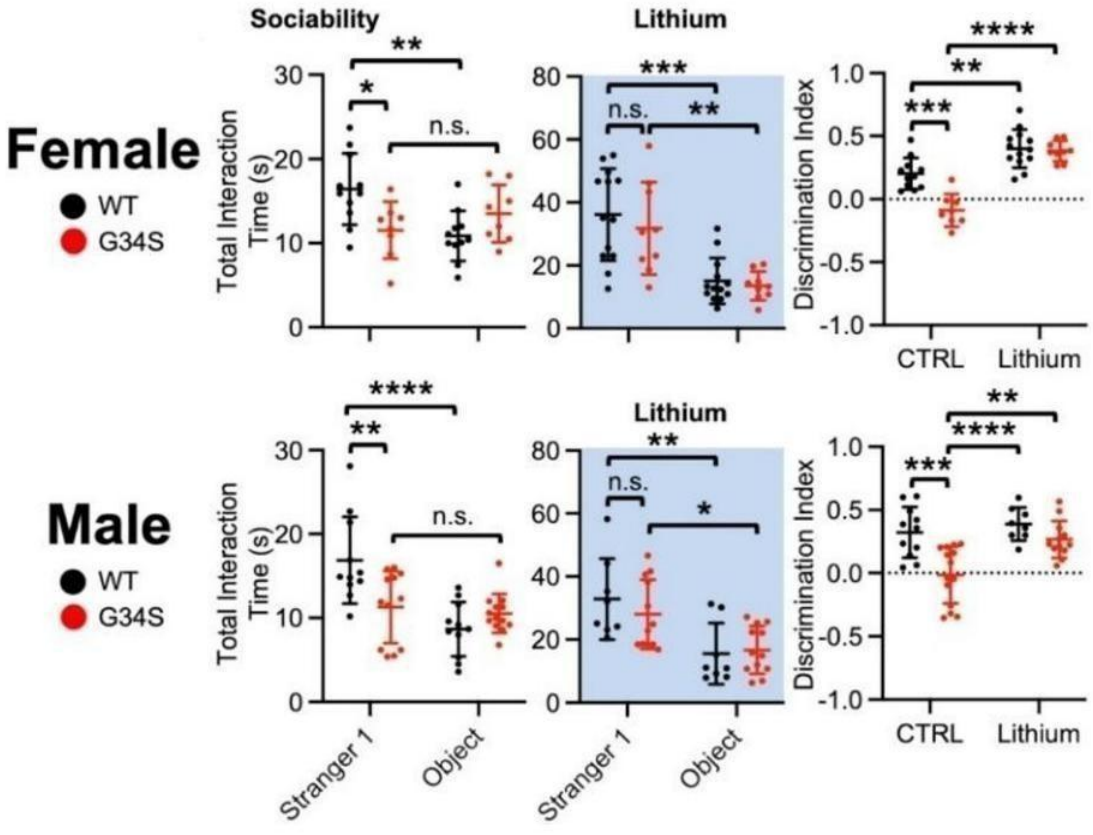

Figure 5. δ-catenin G34S induces social dysfunction in mice in sociability test, which is reversed by GSK3β inhibition.

Total interaction time and the discrimination index of sociability in female and male mice in each genotype in control and lithium treated conditions (highlighted in light blue) in the three-chamber test (n = number of animals, WT female + standard chow = 11, WT female + lithium chow = 9, G34S female + standard chow = 8, G34S female + lithium chow = 7, WT male + standard chow =11, WT male + lithium chow = 8, G34S male + standard chow = 14, and G34S male + lithium chow = 12, *P < 0.05, **P < 0.01, ***P < 0.001, and ****P < 0.0001, Two-way ANOVA with Tukey test. n.s. indicates no significant difference). Mean ± SD. Experiments performed in collaboration with Hadassah Mendez-Vazquez.

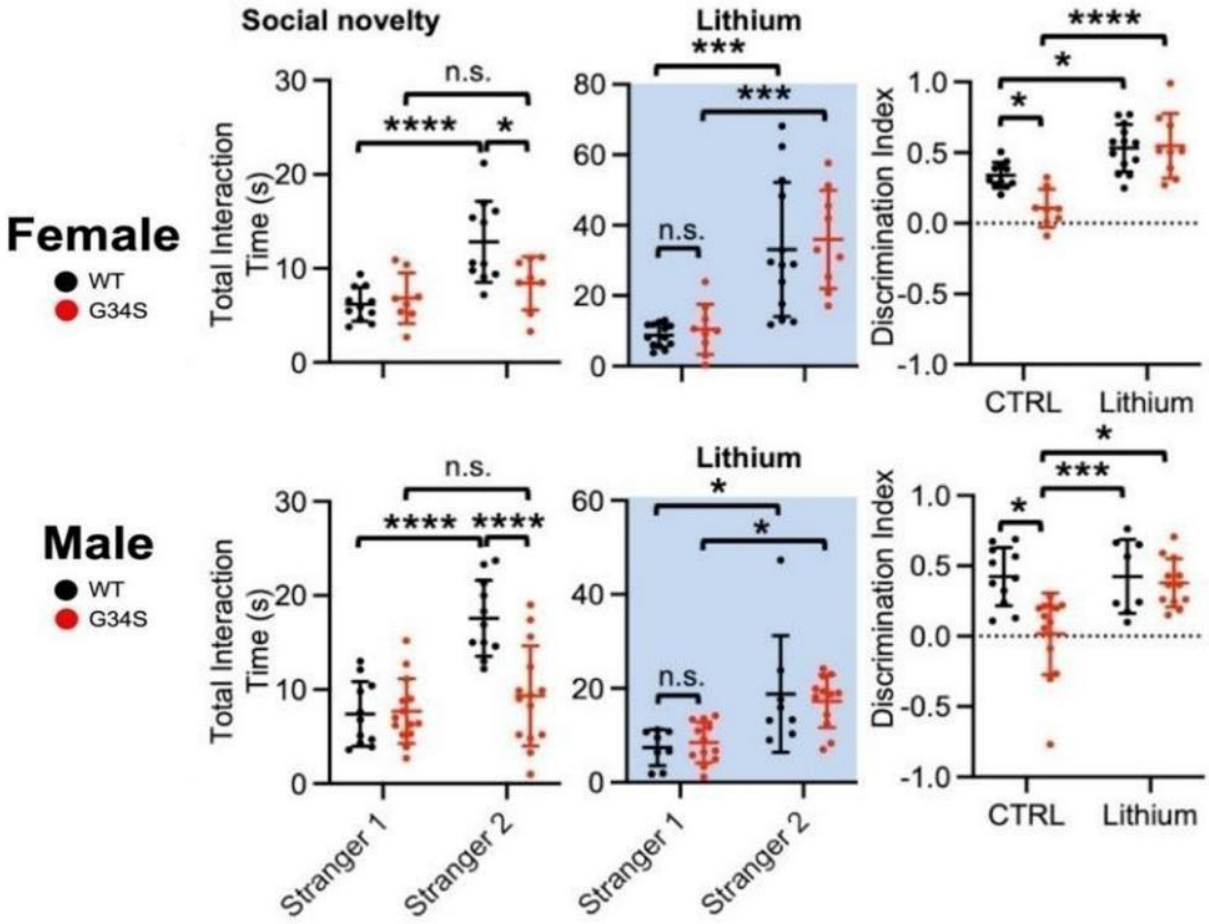

Figure 6. δ-catenin G34S induces social dysfunction in mice in social novelty test, which is reversed by GSK3β inhibition.

Total interaction time and the discrimination index of sociability in female and male mice in each genotype in control and lithium treated conditions (highlighted in light blue) in the three-chamber test (n = number of animals, WT female + standard chow = 11, WT female + lithium chow = 9, G34S female + standard chow = 8, G34S female + lithium chow = 7, WT male + standard chow =11, WT male + lithium chow = 8, G34S male + standard chow = 14, and G34S male + lithium chow = 12, *P < 0.05, **P < 0.01, ***P < 0.001, and ****P < 0.0001, Two-way ANOVA with Tukey test. n.s. indicates no significant difference). Mean ± SD. Experiments performed in collaboration with Hadassah Mendez-Vazquez.

To further examine the social deficit observed in G34S mutant mice, we performed a reciprocal social interaction test before and after lithium treatment (**Figure 7**). Consistent with our findings in the three-chamber test, a significant social deficit was observed in the G34S mutant mice, as both male and female G34S mice had a significant decrease in their frequency and duration of contacts as compared to WT littermates (**Figure 7**). However, this deficit is reversed through the use of lithium treatment in male and female δ-catenin G34S mice (**Figure 7**). This further shows the social dysfunction observed in mice with the δ-catenin G34S mutation, of which can be restored through the pharmacological inhibition of GSK3β activity.

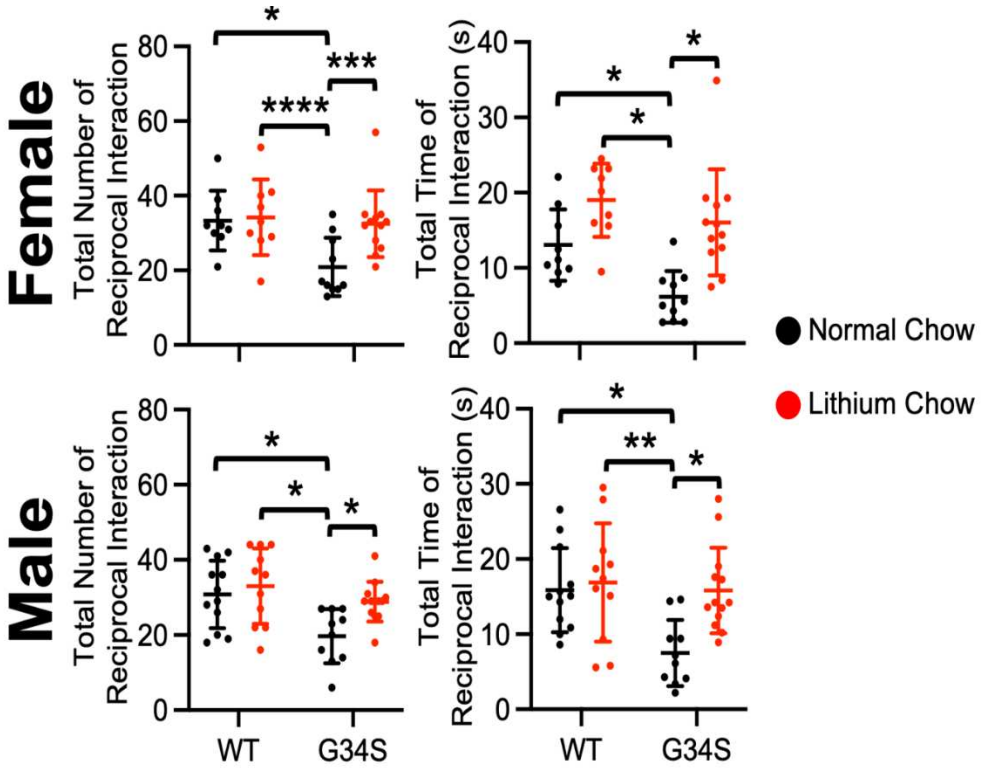

Figure 7. Social dysfunction in δ-catenin G34S mice in reciprocal social interaction test.

The results of the total number of contacts and total duration of contacts in WT and δ-catenin G34S mice in the social interaction test (n=9 WT and 10 G34S control females and 12 WT and 10 G34S control males, as well as n=9 WT and 12 G34S lithium-treated females and 11 WT and 13 G34S lithium treated males, **p*<0.05, ***p*<0.01, ****p*<0.001, and *****p*<0.0001, Two-way ANOVA with Tukey test). Mean ± SD.

δ-Catenin G34S Mice Show Normal Olfaction, Anxiety Levels, and Locomotor Activity.

It is possible that sensory deficits may affect performances in social behavioral assays [52]. During social activity, mice substantially rely on olfaction [52]. The buried food test is a reliable method that depends on the mouse's natural desire to forage using olfactory cues [53]. Thus, we conducted the buried food test to examine whether the δ-catenin G34S mutation affected olfactory functions [52]. We found no significant difference in the latency to find the buried food in δ-catenin G34S female and male mice compared to WT littermates (**Figure 8**), suggesting that δ-catenin G34S mice have normal olfaction. Anxiety levels can also affect social behavior in animals [54, 55]. We thus measured locomotor activity and anxiety-like behavior using the open-field test. We found no significant difference between genotype groups regardless of sex in total traveled distance (locomotor activity) and time spent outside and inside (anxiety-like behavior) (**Figure 8**) This indicates that δ-catenin G34S mice have normal locomotor activity and anxiety levels, whereby the altered behavior observed in the three-chamber test (**Figure 5 andFigure *6***) strongly implies social dysfunction.

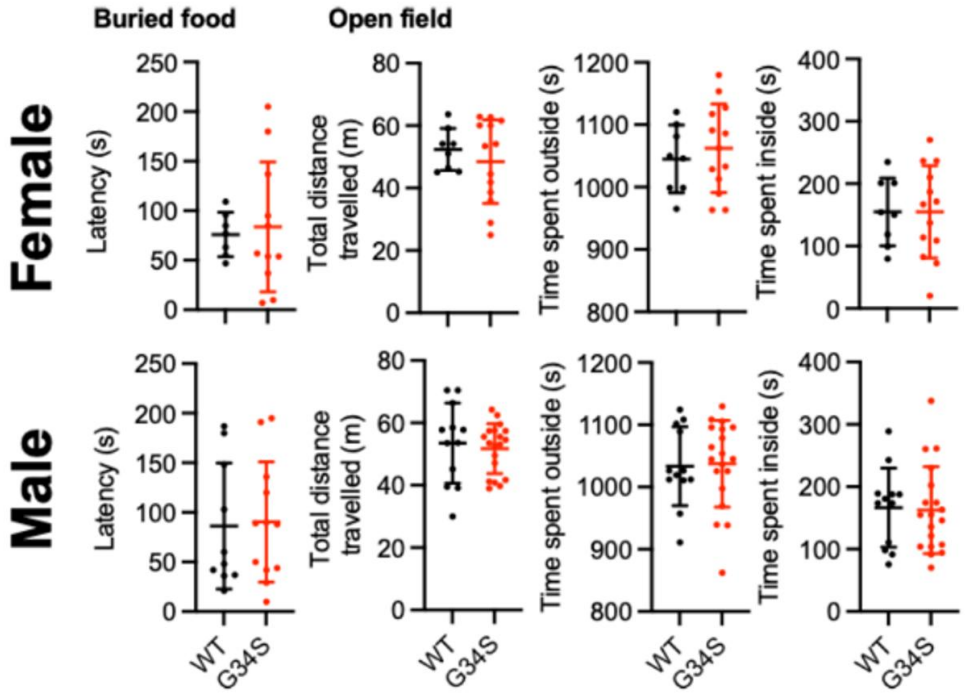

Figure 8. Normal olfaction, locomotor activity, and anxiety levels in δ-catenin G34S mice.

The results of the buried food test in females (n = 7 WT and 11 G34S mice) and males (n = 10 WT and 12 G34S mice). The results of the open field test measuring total distance travelled and time spent outside and inside females (n = 8 WT and 13 G34S mice) and males (n = 12 WT and 19 G34S mice). Mean ± SD. Experiments performed in collaboration with Hadassah Mendez-Vazquez.

A Significant Reduction of Synaptic GluA2 in the δ-Catenin KO Cortex and Altered Glutamatergic Activity in Cultured δ-Catenin KO Cortical Neurons.

We additionally generated δ-catenin KO mice to further confirm whether the loss of δ-catenin functions was important for glutamatergic activity in cortical neurons and social behavior in animals [52]. We examined if δ-catenin KO affected synaptic AMPAR levels in the brain. The PSD fractions of the cortex were collected from 3-month-old female and male WT and KO animals to analyze for synaptic AMPAR levels as shown in Error! Reference source not found. W hen compared to the WT cortex, we found no difference in synaptic GluA1 levels but a significant reduction in GluA2 levels in the female and male KO animals' cortices (**Figure 9**Error!

Reference source not found. **A and 9B**), as seen in the G34S mouse cortex (**Figure 3**). This suggests that the loss of δ-catenin expression in mice significantly reduces synaptic GluA2 levels selectively in the cortex, which likely alters AMPAR-mediated glutamatergic activity in the δ-catenin KO cortex, like the G34S cortex.

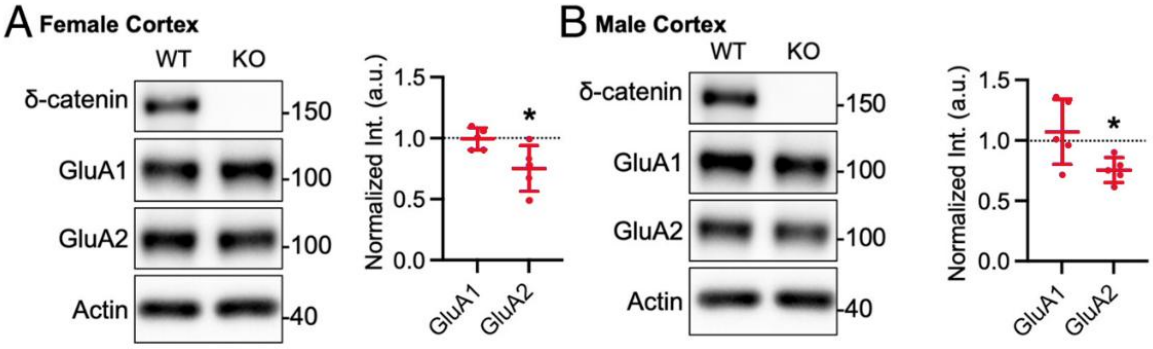

Figure 9. A significant reduction of synaptic GluA2 in the δ-catenin KO cortex.

Representative immunoblots and summary graphs of normalized GluA1 and GluA2 levels in the cortical PSD fractions from WT and δ-catenin KO **(A)** female and **(B)** male mice (n = 5 immunoblots from 3 mice in each condition, Kruskal-Wallis test with Dunn's test, *P < 0.05). The position of molecular mass markers (kDa) is shown on the right of the blots. Mean ± SD.

With this, we conducted Ca^{2+} imaging with glutamate uncaging in cultured WT and δ-catenin KO mouse cortical neurons to determine whether δ-catenin KO altered glutamatergic activity in excitatory and inhibitory cortical neurons as shown in **Figure 4A and 4B**. Glutamate-induced Ca^{2+} activity was markedly elevated in cultured 12 to 14 DIV mouse excitatory cortical δ-catenin KO neurons compared to WT cells (**Figure 10A**). Conversely, glutamatergic activity in cultured KO inhibitory interneurons was significantly lower than WT cells (**Figure 10B**). This suggests that glutamatergic activity in δ-catenin KO excitatory and inhibitory cells is altered in opposite ways, as seen in G34S cortical neurons (**Figure 4A**). To determine if a lack of δ-catenin was the cause of the changes observed in δ-catenin KO cortical neurons, we transfected δ-catenin in both the δ-catenin KO and WT cortical neurons. Following transfection

of δ-catenin, glutamatergic activity of both excitatory and inhibitory KO cortical neurons was restored to the activity levels observed in WT cells (**Figure 10 A and B**).

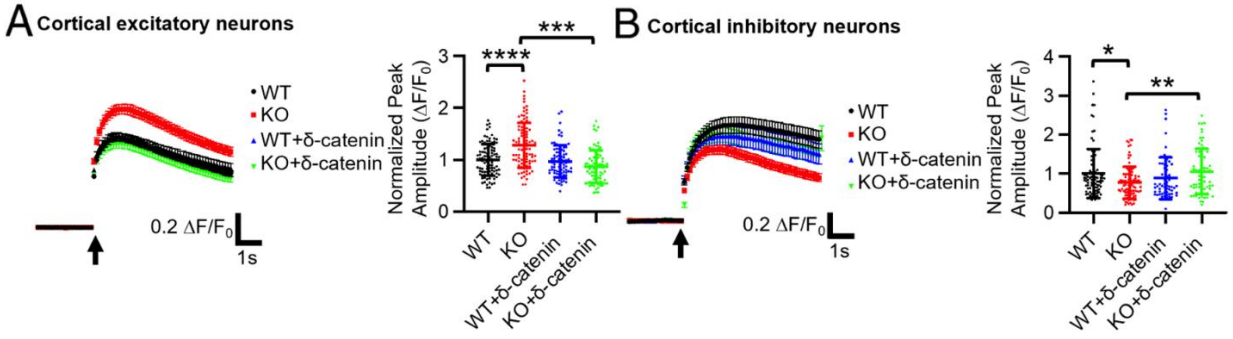

Figure 10. Altered glutamatergic activity in cultured δ-catenin KO cortical neurons.

(A) Average traces of GCaMP7s signals and summary data of normalized peak amplitude in each condition in excitatory neurons (n = number of neurons from 3 independent cultures, WT = 70 and KO = 73). **(B)** Average traces of GCaMP6f signals and summary data of normalized peak amplitude in each condition in inhibitory interneurons (n = number of neurons from three independent cultures, WT = 38 and KO = 30, ***P < 0.01 and ****P < 0.0001, the unpaired two-tailed Student's t test). An arrow indicates photostimulation. Mean ± SD.

Furthermore, we examined if δ-catenin KO additionally affected spontaneous neuronal activity in KO cortical neurons (**Figure 11**) [52]. Consistent with the results observed in glutamatergic activity of δ-catenin KO cortical neurons, neuronal activity was significantly higher in excitatory cortical δ-catenin KO neurons compared to WT cells, and the neuronal activity of cultured KO inhibitory neurons was significantly lower than WT cells (**Figure 11**). Comparable to the changes observed in the glutamatergic activity of KO cells, neuronal activity was restored in both excitatory and inhibitory δ-catenin KO cortical neurons when transfected with δ-catenin (**Figure 11**). This suggests that δ-catenin deficiency is the direct cause of the glutamatergic and neuronal changes observed in δ-catenin KO cells.

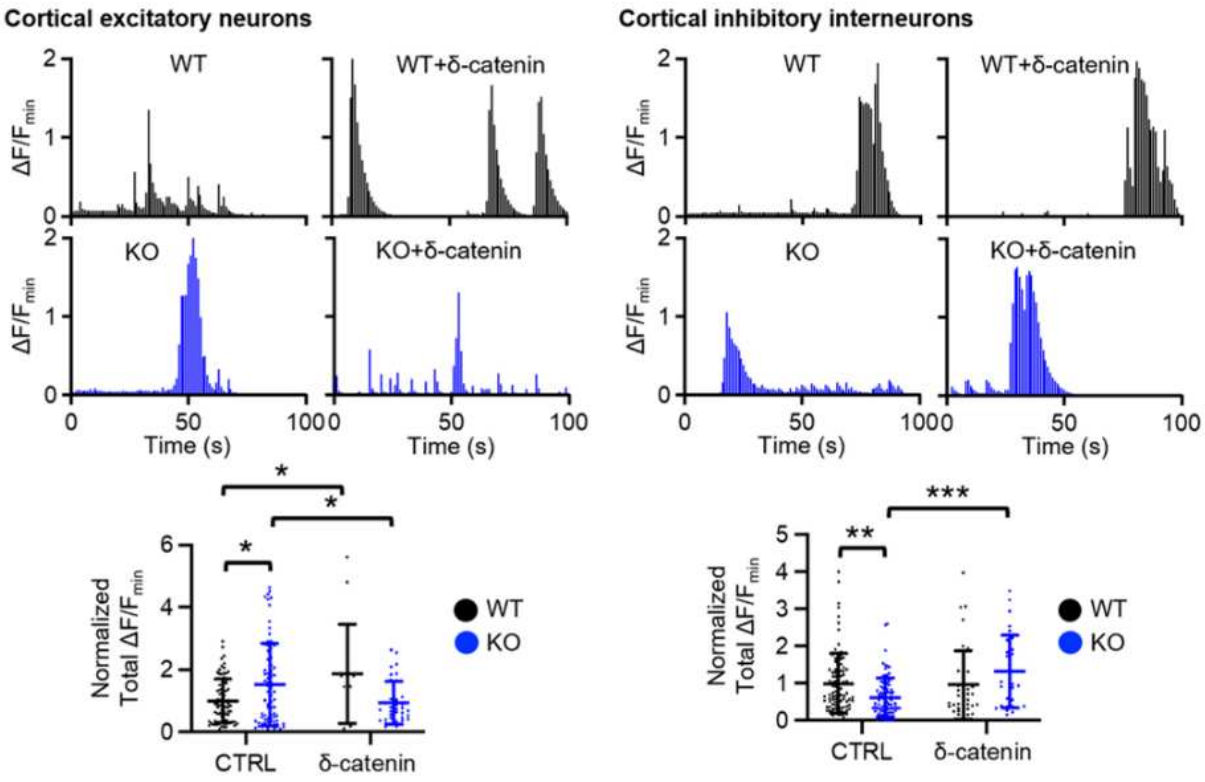

Figure 11. Altered spontaneous neuronal activity in KO cortical neurons.

Traces of transfected Gcamp6f signals in excitatory and inhibitory cells and summary data of normalized total calcium activity in each condition (n = 79 WT CTRL, 77 KO CTRL. 25 WT + d-cat, 37 KO + d-cat). Experiments performed by Seonil Kim.

Abnormal Social Behavior in δ-Catenin KO mice.

We used the three-chamber test to determine whether the loss of δ-catenin expression affected social behavior in mice (

Figure *12* and Figure 13) [52]. In the sociability test, WT female and male mice interacted significantly longer with stranger 1 than a novel object, showing normal sociability (

Figure *12*). However, in δ-catenin KO female and male mice, no significant difference in total interaction time was found between stranger 1 and the novel object (

Figure *12*). Importantly, social interaction with stranger 1 in δ-catenin KO female and male mice was markedly lower than WT mice (

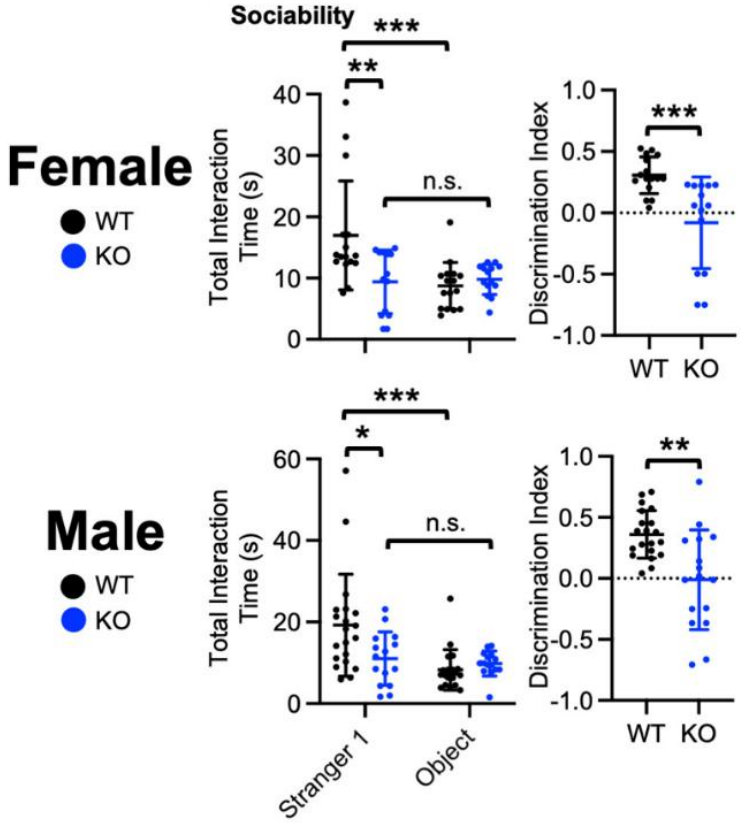

Figure *12*).

Figure 12. δ-catenin KO induces social dysfunction in mice in sociability test.

Total interaction time and the discrimination index of sociability in female and male WT and KO mice in the three-chamber test (n = number of animals, WT female = 16, KO female = 14, WT male = 20, and KO male = 15, *P < 0.05, **P < 0.01, ***P < 0.001, and ****P < 0.0001, For total interaction time, Two-way ANOVA with Tukey test was used. For the discrimination index, the unpaired two-tailed Student's t test was used. n.s. indicates no significant difference). Mean ± SD. Total interaction time and the discrimination index of sociability in female and male WT and KO mice in the three-chamber test (n = number of animals, WT female = 16, KO female = 14, WT male = 20, and KO male = 15, *P < 0.05, **P < 0.01, ***P < 0.001, and ****P < 0.0001, For total interaction time, Two-way ANOVA with Tukey test was used. For the discrimination index, the unpaired two-tailed Student's t test was used. n.s. indicates no significant difference). Mean ± SD.

In the social novelty test, WT mice interacted with stranger 2 for longer than they did with stranger 1, an indication of normal social novelty preference (**Figure 13**). Conversely, there was no significant difference in reciprocal sniffing time between stranger 1 and stranger 2 in δ-catenin KO female and male mice (**Figure 13**). Compared to WT animals, social interaction with stranger 2 was significantly lower in both female and male δ-catenin KO mice (**Figure 13**). Moreover, the discrimination index confirmed that δ-catenin KO disrupted social behavior in female and male mice (

Figure *12* and Figure 13). These findings indicate that δ-catenin KO mice exhibit abnormal sociability and social novelty preference in the three-chamber test similar to that of δ-catenin G34S mice (**Figure 5 and Figure *6***).

Figure 13. δ-catenin KO induces social dysfunction in mice in social novelty test.

Total interaction time and the discrimination index of social novelty in female and male WT and KO mice in the three-chamber test (n = number of animals, WT female = 16, KO female

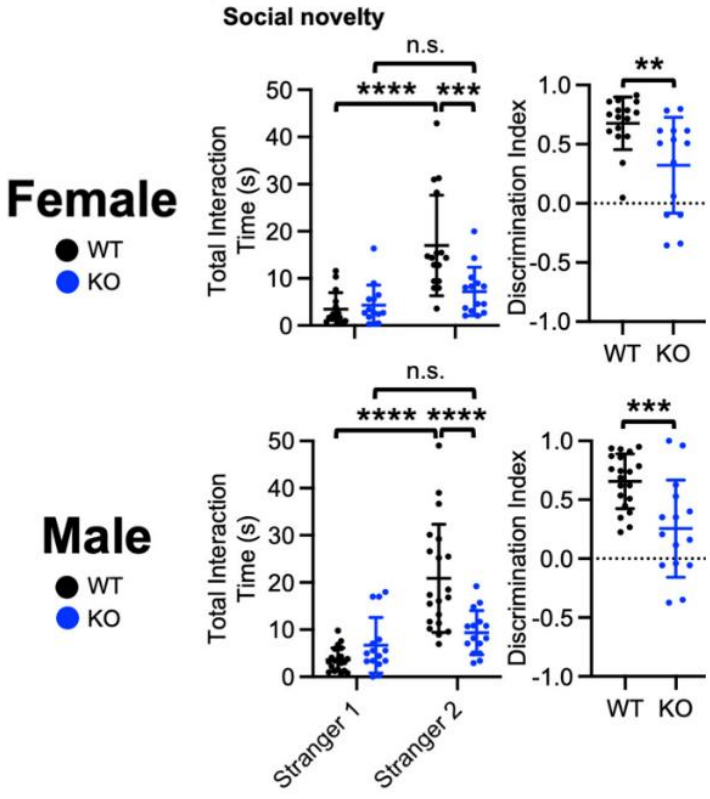

= 14, WT male = 20, and KO male = 15, *P < 0.05, **P < 0.01, ***P < 0.001, and ****P < 0.0001, For total interaction time, Two-way ANOVA with Tukey test was used. For the discrimination index, the unpaired two-tailed Student's t test was used. n.s. indicates no significant difference). Mean ± SD. Total interaction time and the discrimination index of social novelty in female and male WT and KO mice in the three-chamber test (n = number of animals, WT female = 16, KO female = 14, WT male = 20, and KO male = 15, *P < 0.05, **P < 0.01, ***P < 0.001, and ****P < 0.0001, For total interaction time, Two-way ANOVA with Tukey test was used. For the discrimination index, the unpaired two-tailed Student's t test was used. n.s. indicates no significant difference). Mean ± SD.

To further assess the social behavior of the δ-catenin KO mice, we administered an unrestricted social interaction test (**Figure 14**). In this test, consistent with the results observed in our G34S mutant mice (**Figure 7**) we found that both the frequency and duration of social interaction was significantly lower in both female and male δ-catenin KO mice compared to WT mice.

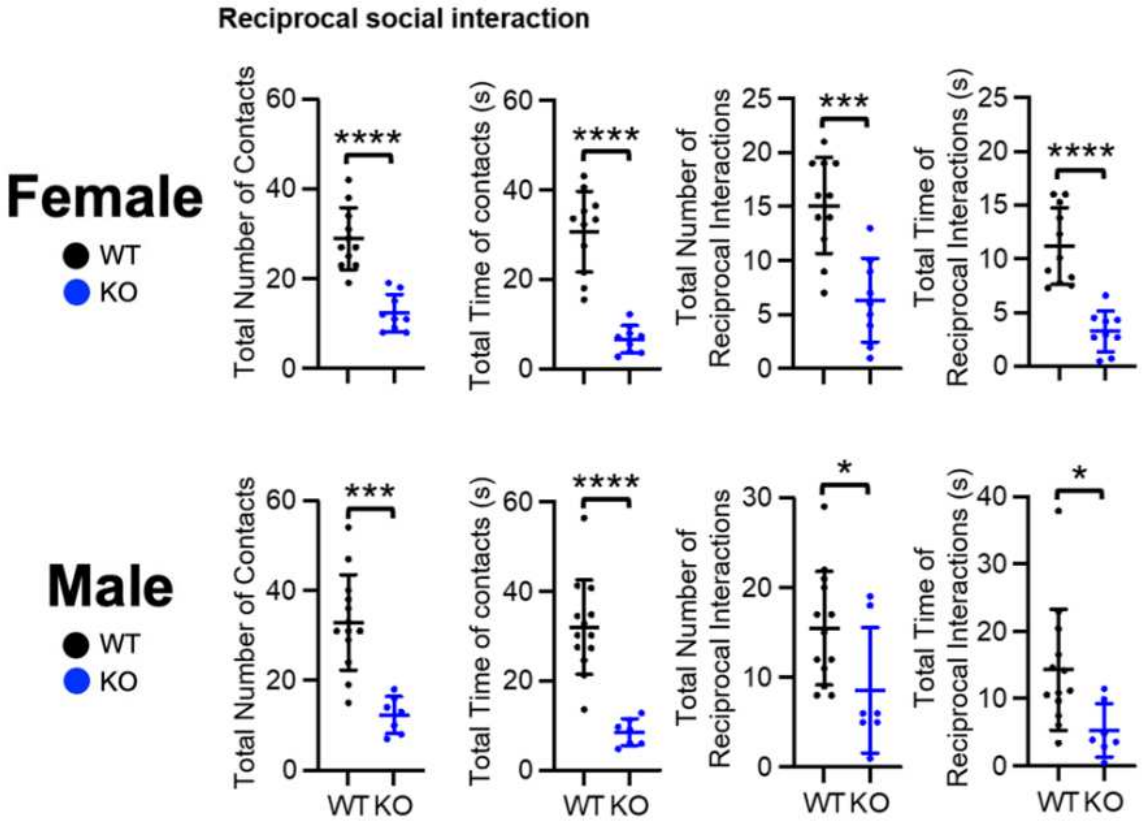

Figure 14. δ-catenin KO induces social dysfunction in mice in reciprocal social interaction test.

The results of the total number of contacts, total duration of contacts, total number of reciprocal interactions, and total duration of reciprocal interactions in WT and δ-catenin KO mice in the reciprocal social interaction test (n = number of animals, WT female = 11, KO female = 9, WT male = 13, and KO male = 7, *p < 0.05, ***p < 0.001, and ***p < 0.001, two-tailed unpaired student's t-test). Mean ± SD.

δ-Catenin Is Required for Lithium-Induced Restoration of Normal Social Behavior in G34S Mice.

We used δ-catenin KO mice to address whether δ-catenin was required for lithium effects on social behavior [52]. We fed δ-catenin KO mice with lithium chow and conducted the three-chamber test and compared their social behavior to that of lithium-treated δ-catenin G34S animals. In the sociability test, we found no significant difference in total interaction time between stranger 1 and the novel object in lithium-treated δ-catenin KO female and male mice, an indication of abnormal sociability, whereas we found normal sociability in lithium-treated δ-catenin G34S animals (**Figure 15**). Importantly, social interaction with stranger 1 in δ-catenin

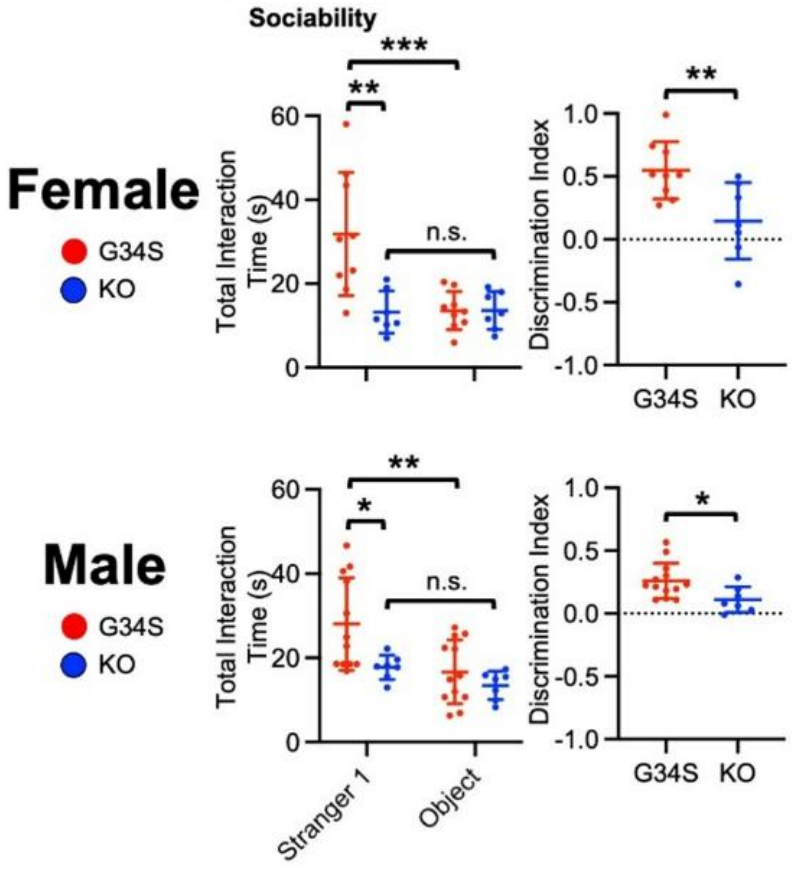

KO female and male mice was markedly lower than G34S mice following lithium treatment (**Figure 15**).

Figure 15. δ-catenin is required for lithium-induced restoration of normal social behavior in G34S mice in sociability test.

Total interaction time and the discrimination index of sociability in lithium-treated female and male G34S and KO mice in the three-chamber test (n = number of animals, G34S female + lithium = 9, KO female + lithium = 7, G34S male + lithium = 12, and KO male + lithium = 7, *P < 0.05, **P < 0.01, ***P < 0.001, and ****P < 0.0001, For total interaction time, Two-way ANOVA with Tukey test was used. For the discrimination index, the unpaired two-tailed Student's t test was used. n.s. indicates no significant difference). Mean ± SD. Experiments performed in collaboration with Hadassah Mendez-Vazquez.

In the social novelty test, after lithium was administered, there was no significant difference in reciprocal sniffing time between stranger 1 and stranger 2 in δ-catenin KO female and male mice, an indication of abnormal social novelty preference, while G34S female and male animals exhibited normal social novelty preference following lithium treatment (**Figure 16**).

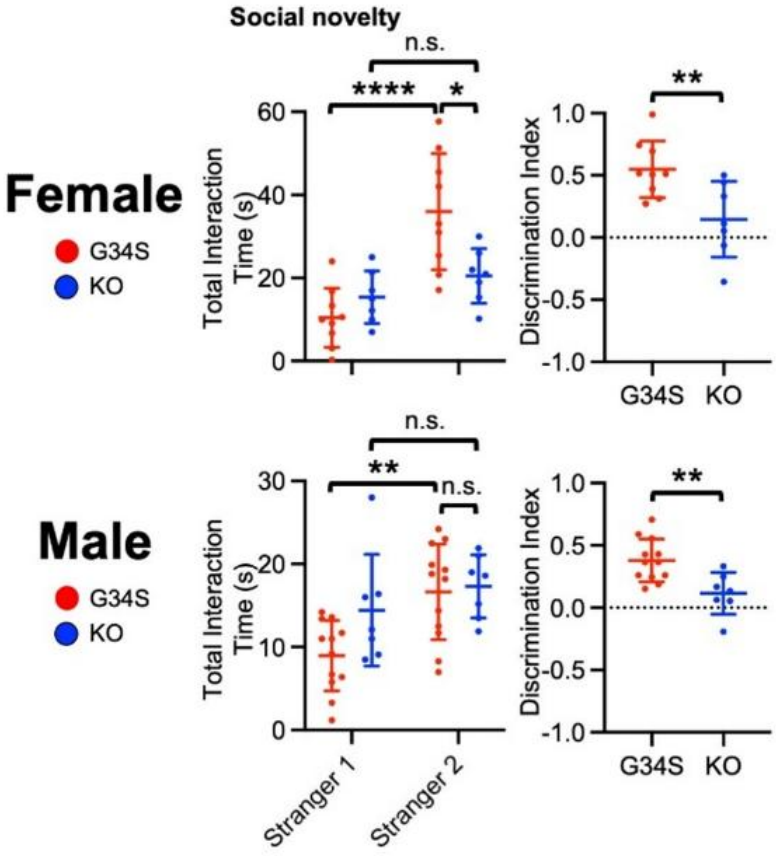

Finally, the discrimination index revealed that lithium was unable to restore normal sociability and social novelty preference in δ-catenin KO female and male mice unlike δ-catenin G34S animals (**Figure 15 and Figure *16***). These findings suggest that δ-catenin is required for lithium-induced restoration of normal social behavior in δ-catenin G34S mice.

Figure 16. δ-catenin is required for lithium-induced restoration of normal social behavior in G34S mice in social novelty test.

Total interaction time and the discrimination index of social novelty in lithium-treated female and male G34S and KO mice in the three-chamber test (n = number of animals, G34S female + lithium = 9, KO female + lithium = 7, G34S male + lithium = 12, and KO male + lithium = 7, *P < 0.05, **P < 0.01, ***P < 0.001, and ****P < 0.0001, For total interaction time, Two-way ANOVA with Tukey test was used. For the discrimination index, the unpaired two-tailed Student's t test was used. n.s. indicates no significant difference). Mean ± SD. Experiments performed in collaboration with Hadassah Mendez-Vazquez.

δ-Catenin KO Mice Show Normal Olfaction, Anxiety Levels, and Locomotor Activity.

As is the case with our δ-catenin G34S mutant mice, it is possible that the deleterious mutation present in our KO mice causes sensory deficits that could alter the performance of our test mice buring behavioral assays [54]. Because of this, we performed the buried food and open field tests that were previously performed on the δ-catenin G34S mice (**Figure 8**) on the δ-catenin KO mice as well to assess their olfactory sense, anxiety levels, and locomotor activity. We found that δ-catenin KO female and male mice showed normal olfactory function in the buried food test, having no significant differences in their test results as compared to WT littermates (

Figure 17). Finally, the open-field test showed normal locomotor activity and anxiety levels in δ-catenin KO female and male mice, once again with no significant differences in their test results when compared to WT littermates (

Figure 17). Combined with the other data from my thesis work (

Figure *12*-14), we conclude that δ-catenin KO mice exhibit abnormal social behavior in the three-chamber test without altered olfaction, locomotor activity, and anxiety-like behavior.

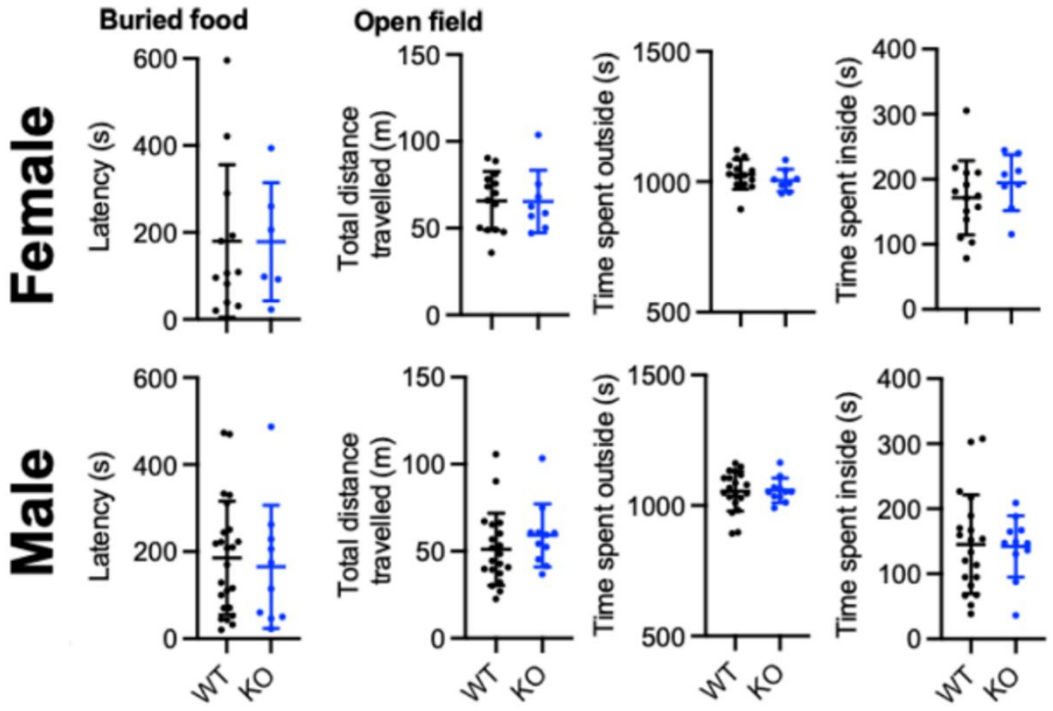

Figure 17. Normal olfaction, locomotor activity, and anxiety levels in δ-catenin KO mice.

The results of the buried food test in females (n = 12 WT and 6 KO mice) and males (n = 24 WT and 10 KO mice). The results of the open field test measuring total distance travelled and time spent outside and inside in females (n = 18 WT and 8 KO mice) and males (n = 20 WT and 11 KO mice). Mean ± SD. Experiments performed in collaboration with Hadassah Mendez-Vazquez.

δ-catenin Deficiency Induces Altered Prefrontal Oscillations in the Medial Prefrontal Cortex.

Lastly, we used G34S mutant mice to examine prefrontal oscillations. We used the δ-catenin G34S mutant mice to determine if neural oscillations were restored alongside social behavior via lithium treatment. We performed stereotaxic surgery on WT and G34S mutant mice

to insert electrodes into the mPFC. After the surgical site had healed, both WT and G34S mutant mice were placed in an unrestricted social interaction test with non-littermate WT mice. During reciprocal interaction, female and male G34S mutant mice had significantly higher theta power than WT mice (**Figure 18A**). In addition, female mice G34S mutant mice showed a significant increase in gamma power, whereas gamma power was significantly lower in male G34S mutant mice as compared to WT mice (**Figure 18B**). However, each of these changes in the oscillatory powers for the G34S mutant mice were reversed by lithium treatment (**Figure 18 A and 18B**). This suggests that the difference in the oscillatory powers found in the δ-catenin mutant mPFC contributes to social dysfunction in the G34S mouse model.

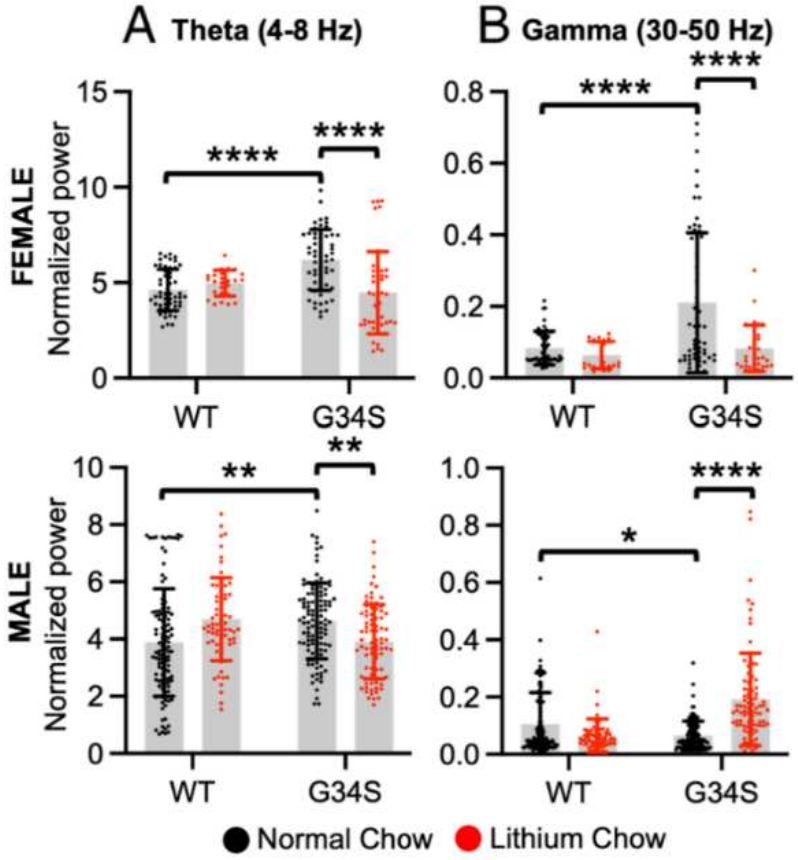

Figure 18. δ-catenin deficiency induces altered prefrontal oscillations in the medial prefrontal cortex.

Summary graphs of the normalized power of prefrontal **(A)** theta powers (4-8 Hz) and **(B)** gamma (30-50 HZ) during reciprocal social interaction for female and male mice (n = number of channels [number of animals], Female; WT + normal chow=54 [4], G34S + normal chow=58 [5], WT + lithium chow=26 [2], and G34S + lithium chow = 45 [4] and Male; WT + normal chow =

115 [10], G34S + normal chow = 112 [9], WT + lithium chow = 67 [5], and G34S + lithium chow = 83 [7]). *p<0.05, **p<0.01, and ****p<0.0001. Two-way ANOVA with Tukey test. Mean ± SD.

DISCUSSION[1]

ASD is a multifactorial neurodevelopmental disorder characterized by impaired social communication, social interaction, and repetitive behaviors [56]. The pathophysiology of ASD is largely influenced by strong genetic components throughout the early stages of development [56]. The Simmons Foundation Autism Research Initiative (SFARI) gene database (https://gene.sfari.org) reports more than 1,000 candidate genes and copy number variations (CNVs) loci associated with ASD. Many of these ASD candidate genes are implicated in synaptic formation and function [57]. In fact, several molecular, cellular, and functional studies of ASD experimental models suggest that synaptic abnormalities underlie ASD pathogenesis (known as synaptopathy) [58]. However, the mechanisms by which these gene products induce synaptopathy and ASD symptoms are not completely understood. The *δ-catenin* gene is strongly associated with ASD according to multiple human genetic studies [27, 30, 31, 33]. Notably, the ASD-associated G34S mutation in the *δ-catenin* gene induces a loss of δ-catenin functions in excitatory synapses [33]. However, how the ASD-associated δ-catenin missense mutation causes the loss of δ-catenin functions to contribute to ASD synaptopathy remains unclear. Our previous study used neuroblastoma cells to identify that the ASD-associated δ-catenin G34S mutation enhances δ-catenin degradation, which is completely reversed by the reduction of GSK3β activity. In my thesis work using two mouse models – δ-catenin G34S knockin and δ-catenin KO – we further identify that the δ-catenin deficiency alters cortical glutamatergic E/I at the cellular levels and disrupts social behavior (**Figure 4A and 4B**). We also show that δ-catenin is required for lithium-induced restoration of normal social behavior in δ-catenin G34S mice (**Figure 15 and Figure *16***). With this, we also investigated if a significant

change is observed in δ-catenin KO mice before and after lithium treatment and found that there is no significant difference in δ-catenin KO social behavior (**Figure 19**). As the expression of δ-catenin is highly correlated with other ASD-risk genes that are involved in synaptic structure and function [40, 45-47], our findings can help us better understand ASD synaptopathy. Finally, we discover that prefrontal network activity during social interaction is significantly altered in ASD mutant mice, which likely contributes to social dysfunction. Importantly, pharmacological inhibition of GSK3β activity can reverse these changes in G34S mice (**Figure 3**). Taken altogether, my work reveals that the loss of δ-catenin functions arising from the ASD-associated

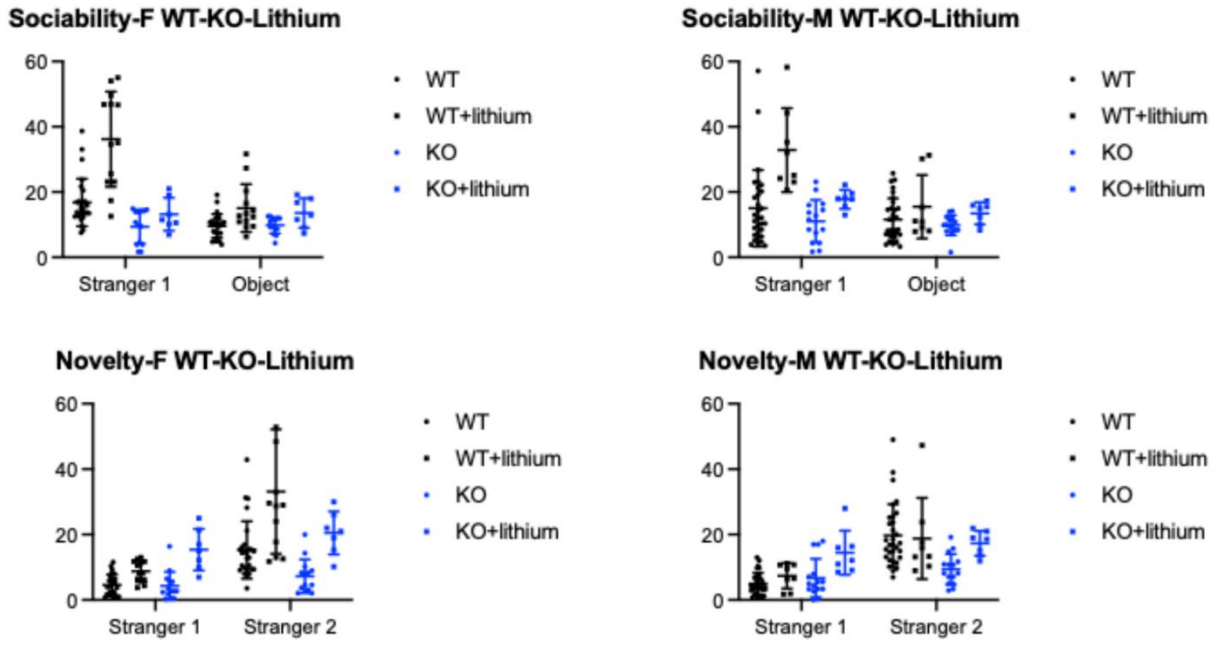

G34S mutation induces social dysfunction via alterations in activity at the synaptic, cellular, and network levels and that GSK3β inhibition can reverse δ-catenin G34S-induced synaptic, behavioral, and oscillatory deficits.

Figure 19. Lithium treatment has no effect on behavior of δ-catenin KO mice.

Total interaction time of sociability and social novelty tests in female and male mice in each genotype (WT and KO) in control and lithium treated conditions (KO+lithium, WT+lithium) in the three-chamber behavioral assay.

With assistance from my former and current colleagues, we have shown that the loss of δ-catenin functions in the G34S mutation and KO has similar opposing effects on glutamatergic activity in cortical excitatory and inhibitory cells (**Figure 4. Altered glutamatergic activity in cultured G34S cortical neurons.**

A and 4B). However, it remains unclear how the loss of δ-catenin functions differentially affects cellular excitation and inhibition. GluA2-containing AMPARs are Ca^{2+} impermeable, whereas GluA2-lacking AMPARs are Ca^{2+} permeable and have high single channel conductance [59]. Cortical excitatory neurons have no basal Ca^{2+}-permeable AMPAR (CP-AMPAR) expression, while cortical inhibitory interneurons contain GluA2-lacking CP-AMPARs [60]. Therefore, δ-catenin G34S and KO-induced reduction of GluA2 in excitatory cells may promote the synaptic expression of highly conductive GluA2-lacking CP-AMPARs, which contributes to higher glutamatergic and neuronal activity. In fact, former Kim lab members have identified that increased glutamatergic activity measured by Ca^{2+} imaging with glutamate uncaging in δ-catenin G34S excitatory cells is significantly decreased when we treat with the CP-AMPAR blocker, NASPM [51], which supports our idea. Conversely, in δ-catenin G34S and KO inhibitory interneurons, GluA1/2 or GluA2/3 heteromeric AMPARs are likely decreased, which leads to an overall decrease in glutamatergic and neuronal activity. Research suggests that GluA2 is expressed in most cortical inhibitory interneurons, which is likely affected by δ-catenin deficiency in our study, although it is considerably lower in cortical interneurons than pyramidal neurons [61-65]. This suggests that while δ-catenin deficiency lowers synaptic GluA2 levels in cortical neurons, it has the opposite effects on glutamatergic and neuronal activity in excitatory and inhibitory cells, potentially altering the E/I balance. Alternatively, extrasynaptic glutamatergic receptors may play important roles in altered glutamatergic activity in δ-catenin G34S cells. Several extrasynaptic AMPARs and NMDA receptors (NMRARs) are expressed on the plasma membrane of neurons, and it is known that these receptors function differently from those

directed at the PSD [66]. Specifically, a small number of CP-AMPARs are in extrasynaptic areas where they can be rapidly recruited to synapses during synaptic plasticity [67, 68]. Therefore, it is possible that δ-catenin deficiency affects glutamatergic activity via these receptor populations. Another explanation is that the loss of synaptic GluA2 leads to a reduction of excitability in δ-catenin deficiency inhibitory neurons, which results in less synaptic inhibition in glutamatergic neurons and thus an increase of neuronal activity in these cells (disinhibition). Notably, a recent study shows that the loss of δ-catenin functions induced by shRNA-mediated δ-catenin knockdown significantly decreases cortical neurons' inhibition to increase excitation [40]. Research also suggests that parvalbumin-positive (PV+) inhibitory interneurons in the medial prefrontal cortex (mPFC) receive direct glutamatergic inputs from the ventral hippocampus, mediodorsal thalamus, and basolateral amygdala to drive feedforward inhibition onto prefrontal pyramidal neurons, which is important for the regulation of social behavior [13, 14, 17, 69-71]. Hence, δ-catenin may be important for glutamatergic activity in PV+ inhibitory interneurons to provide feedforward inhibition onto pyramidal neurons in the mPFC, which regulates social behavior. δ-catenin deficiency-induced disinhibition therefore could contribute to the increase in neuronal activity in excitatory cells, particularly in the intact circuits, to cause social dysfunction. Finally, a recent study identifies that δ-catenin also localizes to inhibitory synapses [40]. Therefore, it is possible that δ-catenin deficiency directly affects inhibitory synapses to change E/I ratio. In conclusion, there are still many important questions surrounding the molecular mechanisms of how δ-catenin deficiency affects E/I ratio that the findings of my thesis work allow us to get closer to an answer for.

Pharmacological treatment of ASD is challenging, due in large part to the heterogeneity in the presentation of ASD [72]. Existing therapies aim to treat specific symptoms, rather than address the basic underlying etiologies [73]. Thus, areas of research focusing on therapeutic agents that directly target the underlying pathology of ASD are an important current and future

need. Recent studies suggest that GSK3β activity is strongly implicated in the pathophysiology of ASD [74-81]. However, extensive studies have yielded inconsistent data on the role of GSK3β activity in the molecular and behavioral effects. For example, elevated GSK3β activity is responsible for the ASD-related phenotypes in the mouse model of fragile X mental retardation (FMR) [74-77]. Conversely, inactivation of GSK3β is associated with the ASD-related phenotypes found in deletion of the *phosphatase and tensin homolog on chromosome ten (PTEN)* gene in mice [78]. Nonetheless, our study identifies GSK3β as the target to complete the synaptic δ-catenin regulatory pathway and recognizes GSK3β as a therapeutic target for limiting the loss of δ-catenin function-induced synaptopathy in ASD. Moreover, we use lithium to demonstrate inhibition of GSK3β activity as a therapeutic target. Lithium reduces GSK3β activity by elevating the Akt-dependent phosphorylation of the GSK3β autoinhibitory residue, serine 9 [82] or by competing with magnesium for enzyme binding [83]. Interestingly, there is strong evidence that lithium acts as a mood stabilizer through inhibition of GSK3β [84, 85]. Furthermore, one therapeutic action of lithium is the ability to regulate protein stability, in particular synaptic proteins through GSK-3 as one of its targets [82, 86, 87]. The current study demonstrates that lithium can elevate synaptic δ-catenin and GluA2 levels in the cortex and enhance social behavior in mice, which requires δ-catenin expression. In a clinical study of ASD, lithium administration to 30 children and adolescents diagnosed with ASD was shown to improve the symptoms in 43% of patients [88]. Therefore, an increase in δ-catenin levels at synapses by the reduction of GSK3β activity stabilizes synaptic AMPARs and spine integrity, which could be beneficial for ASD. Albeit lithium treatment has shown promising results in my research and that of others [81-83, [88], it is important to understand how lithium works as a therapeutic more generally. Commonly used as a mood stabilizer in disorders such as bipolar disorder [89], lithium is a nonspecific therapeutic, meaning that it does not have any particular target in the body, whereby many aspects of its mechanism of action remain unclear [89]. With this, lithium has been identified to have several adverse or off-target effects in the body when

administered as a form of treatment, such as interference with thyroid hormone production, nephrotoxicity, and cardiac issues like sick sinus syndrome and bradycardia [89]. However, with the experiments performed in my thesis, we identify and clarify an aspect of lithium's targeting in the body through its effects observed on the δ-catenin synaptic protein. Thus, my thesis work allows us to test and better understand a clinically applicable therapeutic protocol for ASD.

Additional interesting findings in my thesis work show a distinction between sexes in the gamma prefrontal oscillations of our G34S mutant mice, wherein female G34S mutant mice had notably higher normalized power than male G34S mutant mice (**Figure 18B**). It is important to acknowledge and consider potential causes of the sex differences present in my thesis work, as they may play an important role in the sex differences observed in human patients with ASD [90], whereby a better understanding of these distinctions could enable us to develop screening methods as well as treatments that have high efficacy in both sexes. A recent study suggests that a general disruption of neural oscillations and overall connectivity are observed in individuals with ASD [91]. This means that both the hyperexcitation and hypoexcitation observed in gamma oscillations within my study are potential indicators/outcomes of ASD. An additional study identifies that neural oscillations are suppressed, or in a hypoexcitatory state, in children with ASD [92], consistent with my findings in our male G34S mutant mice (**Figure 18B**). However, it is important to note that 80% of the subjects within this study were male, with only 20% being female [92]. Overall, the results of my thesis work suggest that there are potential sex differences in the regulation of total δ-catenin and GluA2 expression, given the mechanism of action of the G34S loss-of-function mutation (**Figure 2**). Importantly, studies suggest that δ-catenin and GluA2 levels can be controlled by estrogen signaling [93-95]. More specifically, these previous studies have identified that estrogen signaling can protect against the stress of excessive glutamatergic transmission and alter spine density within the brain [94, 95]. This indicates that δ-catenin and thus GluA2 expression may be differentially regulated based on the

sex of animals, which is an important topic for future research as sex differences in social dysfunction are common, yet not often studied at length [96].

METHODS AND MATERIALS[1]

Animals.

All mice were bred in the animal facility at Colorado State University (CSU). Animals were housed under 12:12 h light/dark cycle. 3-month-old male and female mice were used in the current study. CSU's Institutional Animal Care and Use Committee reviewed and approved the animal care and protocol (3408). δ-catenin G34S mice (RRID:MMRRC_050621-UCD) were generated by Jyothi Arikkath at UNMC Mouse Genome Engineering Core using the CRISPR-Cas9 technique [97]. δ-catenin KO mouse was developed in collaboration with Cyagen Biosciences Inc. utilizing the CRISPR-Cas9 technique [46]. Lithium treatment in animals was conducted as described previously [38]. Lithium animals received standard chow containing 0.17% w/w lithium carbonate (Harlan Teklad) ad libitum for 7 days. Control animals were fed with standard chow.

Primary Cortical Neuron Culture.

Postnatal day 0 (P0) male and female pups from WT, δ-catenin G34S or KO mice were used to produce mouse cortical neuron cultures as shown previously [98, 99]. Heterozygous G34S or KO mice were used to breed for generating each genotype. PCR was performed to identify each genotype before preparing cultures.

GCaMP Ca^{2+} Imaging with Glutamate Uncaging.

We carried out Ca^{2+} imaging with glutamate uncaging in cultured mouse cortical neurons to determine glutamatergic activity as described previously [100]. For Ca^{2+} imaging, a genetically encoded Ca^{2+} indicator, GCaMP, was used. When AAVs of the same serotype are co-infected, many neurons are transduced by both viruses [101]. We thus co-infected AAVs expressing CamK2a-Cre (Addgene #105558-AAV1), pENN.AAV.CamKII 0.4.Cre.SV40 was a

gift from James M. Wilson (Addgene plasmid #105558 ; http://n2t.net/addgene:105558 ; RRID:Addgene_105558), and Cre-dependent GCaMP7s (Addgene #104495-AAV1) [102], pGP-AAV-CAG-FLEX-jGCaMP7s-WPRE was a gift from Douglas Kim & GENIE Project (Addgene plasmid # 104495 ; http://n2t.net/addgene:104495 ; RRID:Addgene_104495), in 4 days *in vitro* (DIV) neurons and imaged 12-13 DIV excitatory neurons. In addition, AAV expressing GCaMP6f under the control of the GABAergic neuron-specific enhancer of the mouse *Dlx* (mDlx) gene (Addgene #83899-AAV1) [103], pAAV-mDlx-GCaMP6f-Fishell-2 was a gift from Gordon Fishell (Addgene plasmid #83899-AAV1 ; http://n2t.net/addgene:83899 ; RRID:Addgene_83899), was infected in 4 DIV neurons and imaged 12-13 DIV inhibitory interneurons. Glass-bottom dishes were mounted on a temperature-controlled stage on an Olympus IX73 microscope and maintained at 37°C and 5% CO_2 using a Tokai-Hit heating stage and digital temperature and humidity controller. For glutamate uncaging, 1 mM 4-methoxy-7-nitroindolinyl (MNI)-caged L-glutamate was added to the culture media, and epi-illumination photolysis (390 nm, 0.12 mW/mm^2, 1 ms) was used to uncage glutamate in the whole field of view. 2 µM TTX was added to prevent action potential-dependent network activity. To block Ca^{2+}-permeable AMPA receptors, 20 µM NASPM was added to the culture media as described previously [98, 104]. A baseline average of 20 frames (10 ms exposure for GCaMP7s and 50 ms exposure for GCaMP6f exposure) (F_0) were captured in the soma prior to glutamate uncaging, and 50 more frames were obtained after single photostimulation. The fractional change in fluorescence intensity relative to baseline ($\Delta F/F_0$) was calculated. The average peak amplitude in the control group was used to normalize the peak amplitude in each cell. The control group's average peak amplitude was compared to the experimental groups' average.

GCaMP Ca^{2+} Imaging

In addition to glutamate uncaging, we examined whether δ-catenin KO differentially affected spontaneous neuronal activity in cultured cortical excitatory and inhibitory cells. As neuronal Ca^{2+} indicates neuronal activity [105], we measured spontaneous somatic Ca^{2+} activity in cultured 12-14 DIV mouse cortical neurons transfected with GCaMP6f without TTX as described previously [99, 106, 107]. Given that the majority of cells in cortical cultures are excitatory neurons [108], we used the CMV promoter to express GCaMP6f (Addgene# 40755) in excitatory cells as shown previously [107]. We used mDlx-GCaMP6f (Addgene #83899) to measure neuronal activity in cultured inhibitory interneurons. We next examined whether δ-catenin expression reversed the KO effects on neuronal activity in these cells. δ-catenin was expressed by transfection with GCaMP6f in WT (WT + δ-catenin) or KO (KO + δ-catenin) cells, and we measured neuronal activity. A 10 ms exposure time and a total of 100 images were obtained with a one-second interval. F_{min} was determined as the minimum fluorescence value during the imaging. Total Ca^{2+} activity was obtained by 100 values of $\Delta F/F_{min} = (F_t - F_{min}) / F_{min}$ in each image, and values of $\Delta F/F_{min} < 0.1$ were rejected due to potential photobleaching. The average total Ca^{2+} activity in the control group (CTRL) was used to normalize total Ca^{2+} activity in each cell. The control group's average total Ca^{2+} activity was compared to the experimental groups' average as described previously [98, 99, 106, 107, 109, 110].

Animal Behavioral Assays.

To assess social behavior, a three-chamber test was performed with a modification of the previously described method [111], as well as unrestricted social interaction with a focus on reciprocal animal sniffing [112]. The buried food assay was performed as described previously [113]. We measured locomotor activity and anxiety-like behavior using the open-field test as carried out previously [111].

Surgical Procedures.

Mice were anesthetized with intraperitoneal (IP) injections of ketamine (17.5 mg/ml) and xylazine (12.5 mg/ml) solution. The total dose of 10 mg/ml was administered with one injection. The induction of anesthesia was confirmed by the lack of reflex to tail pinching with tweezers. Additional ketamine solution doses of 20µl were administered as needed should the reflex to tail pinching still be present. After anesthetic induction, mice would have their heads shaved from nose to the back of neck and were placed in a Neurostar stereotaxic frame. A scalp incision from nasal bone to occipital bone was made to expose the skull, ending at the lateral end of the frontal bone. A stainless-steel screw soldered to wire wrapping wire and gold pins was placed at the anterior frontal bone to be used as a ground wire. A copper wire bent at 90º with a gold pin at the end not inserted into the skull was placed into the left-medial side of the interparietal bone to be used as a reference. Two multi-channel recording electrodes were placed bilaterally at the medial prefrontal cortex (AP: +1.94mm, -1.94mm, ML: +0.40mm, -0.40mm, DV: -2.5mm) with the Stereodrive application by Neurostar. All electrodes were attached to a connector, and dental acrylic cement was used for fixation of the electrodes and connector. Immediately following operation, mice were injected subcutaneously with buprenorphine hydrochloride (0.3 mg/ml) for pain management. A total dose of 0.10 µl was administered to all mice in one injection. Mice would be placed in a sterile cage on a heating pad until awake (~60 mins), at which point they would be given a plastic weigh boat of hydrogel, food and paper-based enrichment with a clear plastic cage top and a 50 ml centrifuge tube of water and were placed in the designated animal room with appropriate labeling. Mice were not given metal cage tops for their housing to avoid damage to surgical site and electrodes. Data was only analyzed from awake mice with normal locomotor function.

In Vivo Local Field Potential Recording.

7-days post-operation, mice were placed in an open field apparatus to perform unrestricted social interaction assay as previously described. Their post-operation electrodes

were connected to an Intan RHD 16-channel recording headstage which connected to Open Ephys software via a 12-pin RHD data cable connector. Open Ephys was used to record the oscillations of 8 channels bilaterally (16 channels total) in the mPFC.

LFP Analysis.

LFP data were analyzed in MATLAB (The Mathworks Inc.) as described previously [114]. The data were formatted for importation into the Brainstorm platform. Recorded traces were downsampled to 2 kHz and then bandpass filtered between 0.1 and 200 Hz. We applied a notch filter at 60 Hz to reduce powerline artifacts. Awake animals' movement may produce more and stronger artifacts in the recorded data. We thus used Independent Component Analysis (ICA) to remove these artifacts. Power spectral density was calculated by a Fast Fourier Transform (FFT) algorithm. The mean absolute power spectra of the theta (4-8 Hz), slow gamma (30-50 Hz), and fast gamma (50-100 Hz) bands were calculated using Welch's method in the Brainstorm platform. The power of each frequency band was normalized to WT and compared for reciprocal interaction in the unrestricted social behavior assay in WT and G34S mutant mice. For theta-gamma phase amplitude coupling (PAC) analysis, we measured the high-frequency bands modulated by theta bands in epochs with a matched, filtered LFP amplitude envelope. Data were filtered into theta, slow gamma, and fast gamma using a phase-invariant, 2^{nd} order Butterworth characteristic filter (MATLAB function filtfilt.m). The analytic signal for each was computed using the Hilbert Transform (MATLAB function hilbert.m), resulting in instantaneous theta phase and gamma band amplitude. The peaks of the gamma-band amplitudes were defined as local maxima at or exceeding the mean + 1 standard deviation (SD) of the baseline gamma-band amplitude from the Hilbert Transform envelopes. The instantaneous theta phase for each peak was extracted.

Statistical Analysis.

We used the GraphPad Prism 9 software to determine statistical significance (set at $P < 0.05$). Grouped results of single comparisons were tested for normality with the Shapiro–Wilk normality or Kolmogorov–Smirnov test and analyzed using the unpaired two-tailed Student's *t* test when data are normally distributed. Differences between multiple groups were assessed by two-way ANOVA) with the Tukey test or nonparametric Kruskal–Wallis test with Dunn's test. The graphs were presented as mean ± SD.

REFERENCES

1. Ko, J., *Neuroanatomical Substrates of Rodent Social Behavior: The Medial Prefrontal Cortex and Its Projection Patterns.* Front Neural Circuits, 2017. **11**: p. 41.
2. Rapin, I. and R. Katzman, *Neurobiology of autism.* Ann Neurol, 1998. **43**(1): p. 7–14.
3. Abrams, R.C., et al., *Personality disorder symptoms and functioning in elderly depressed patients.* Am J Geriatr Psychiatry, 1998. **6**(1): p. 24–30.
4. Goldberg, J.O. and L.A. Schmidt, *Shyness, sociability, and social dysfunction in schizophrenia.* Schizophr Res, 2001. **48**(2-3): p. 343–9.
5. Association, A.P., *Diagnostic and Statistical Manual of Mental Disorders*. Vol. DSM-5®. 2013: American Psychiatric Pub.
6. Christensen, D. and J. Zubler, *CE: From the CDC: Understanding Autism Spectrum Disorder.* Am J Nurs, 2020. **120**(10): p. 30–37.
7. Christensen, J., et al., *Prenatal valproate exposure and risk of autism spectrum disorders and childhood autism.* JAMA, 2013. **309**(16): p. 1696–703.
8. Shaw, K.A., et al., *Prevalence and Early Identification of Autism Spectrum Disorder Among Children Aged 4 and 8 Years - Autism and Developmental Disabilities Monitoring Network, 16 Sites, United States, 2022.* MMWR Surveill Summ, 2025. **74**(2): p. 1–22.
9. Qin, L., et al., *New advances in the diagnosis and treatment of autism spectrum disorders.* Eur J Med Res, 2024. **29**(1): p. 322.
10. Cruz, S., et al., *Is There a Bias Towards Males in the Diagnosis of Autism? A Systematic Review and Meta-Analysis.* Neuropsychol Rev, 2025. **35**(1): p. 153–176.
11. LeClerc, S. and D. Easley, *Pharmacological therapies for autism spectrum disorder: a review.* P T, 2015. **40**(6): p. 389–97.
12. Rojas, D.C. and L.B. Wilson, *gamma-band abnormalities as markers of autism spectrum disorders.* Biomark Med, 2014. **8**(3): p. 353–68.
13. Sun, Q., et al., *Ventral Hippocampal-Prefrontal Interaction Affects Social Behavior via Parvalbumin Positive Neurons in the Medial Prefrontal Cortex.* iScience, 2020. **23**(3): p. 100894.
14. Felix-Ortiz, A.C., et al., *Bidirectional modulation of anxiety-related and social behaviors by amygdala projections to the medial prefrontal cortex.* Neuroscience, 2016. **321**: p. 197–209.
15. Little, J.P. and A.G. Carter, *Subcellular synaptic connectivity of layer 2 pyramidal neurons in the medial prefrontal cortex.* J Neurosci, 2012. **32**(37): p. 12808–19.
16. Xu, S., et al., *Neural Circuits for Social Interactions: From Microcircuits to Input-Output Circuits.* Front Neural Circuits, 2021. **15**: p. 768294.
17. Ferguson, B.R. and W.J. Gao, *Thalamic Control of Cognition and Social Behavior Via Regulation of Gamma-Aminobutyric Acidergic Signaling and Excitation/Inhibition Balance in the Medial Prefrontal Cortex.* Biol Psychiatry, 2018. **83**(8): p. 657–669.
18. Huang, W.C., Y. Chen, and D.T. Page, *Hyperconnectivity of prefrontal cortex to amygdala projections in a mouse model of macrocephaly/autism syndrome.* Nat Commun, 2016. **7**: p. 13421.
19. Cao, W., et al., *Gamma Oscillation Dysfunction in mPFC Leads to Social Deficits in Neuroligin 3 R451C Knockin Mice.* Neuron, 2018. **98**(3): p. 670.
20. Selimbeyoglu, A., et al., *Modulation of prefrontal cortex excitation/inhibition balance rescues social behavior in CNTNAP2-deficient mice.* Sci Transl Med, 2017. **9**(401).
21. Yizhar, O., et al., *Neocortical excitation/inhibition balance in information processing and social dysfunction.* Nature, 2011. **477**(7363): p. 171–8.
22. Abell, F., et al., *The neuroanatomy of autism: a voxel-based whole brain analysis of structural scans.* Neuroreport, 1999. **10**(8): p. 1647–51.

23. Castelli, F., et al., *Autism, Asperger syndrome and brain mechanisms for the attribution of mental states to animated shapes.* Brain, 2002. **125**(Pt 8): p. 1839–49.
24. Schmitz, N., et al., *Neural correlates of executive function in autistic spectrum disorders.* Biol Psychiatry, 2006. **59**(1): p. 7–16.
25. Brumback, A.C., et al., *Identifying specific prefrontal neurons that contribute to autism-associated abnormalities in physiology and social behavior.* Mol Psychiatry, 2018. **23**(10): p. 2078–2089.
26. Liu, L., et al., *Cell type-differential modulation of prefrontal cortical GABAergic interneurons on low gamma rhythm and social interaction.* Sci Adv, 2020. **6**(30): p. eaay4073.
27. Tuncay, I.O., et al., *Analysis of recent shared ancestry in a familial cohort identifies coding and noncoding autism spectrum disorder variants.* NPJ Genom Med, 2022. **7**(1): p. 13.
28. Nyhus, E. and T. Curran, *Functional role of gamma and theta oscillations in episodic memory.* Neurosci Biobehav Rev, 2010. **34**(7): p. 1023–35.
29. Kuga, N., et al., *Prefrontal-amygdalar oscillations related to social behavior in mice.* Elife, 2022. **11**.
30. Miller, D.E., A. Squire, and J.T. Bennett, *A child with autism, behavioral issues, and dysmorphic features found to have a tandem duplication within CTNND2 by mate-pair sequencing.* Am J Med Genet A, 2020. **182**(3): p. 543–547.
31. Guo, H., et al., *Inherited and multiple de novo mutations in autism/developmental delay risk genes suggest a multifactorial model.* Mol Autism, 2018. **9**: p. 64.
32. Wang, T., et al., *De novo genic mutations among a Chinese autism spectrum disorder cohort.* Nat Commun, 2016. **7**: p. 13316.
33. Turner, T.N., et al., *Loss of delta-catenin function in severe autism.* Nature, 2015. **520**(7545): p. 51–6.
34. Silverman, J.B., et al., *Synaptic anchorage of AMPA receptors by cadherins through neural plakophilin-related arm protein AMPA receptor-binding protein complexes.* J Neurosci, 2007. **27**(32): p. 8505–16.
35. Peifer, M., S. Berg, and A.B. Reynolds, *A repeating amino acid motif shared by proteins with diverse cellular roles.* Cell, 1994. **76**(5): p. 789–91.
36. Takeichi, M., *Cadherins: key molecules for selective cell-cell adhesion.* IARC Sci Publ, 1988(92): p. 76–9.
37. Gilbert, J. and H.Y. Man, *The X-Linked Autism Protein KIAA2022/KIDLIA Regulates Neurite Outgrowth via N-Cadherin and delta-Catenin Signaling.* eNeuro, 2016. **3**(5).
38. Farooq, M., et al., *Lithium increases synaptic GluA2 in hippocampal neurons by elevating the delta-catenin protein.* Neuropharmacology, 2017. **113**(Pt A): p. 426–433.
39. Restituito, S., et al., *Synaptic autoregulation by metalloproteases and gamma-secretase.* J Neurosci, 2011. **31**(34): p. 12083–93.
40. Assendorp, N., et al., *CTNND2 moderates the pace of synaptic maturation and links human evolution to synaptic neoteny.* Cell Rep, 2024. **43**(10): p. 114797.
41. Kosik, K.S., et al., *Delta-catenin at the synaptic-adherens junction.* Trends Cell Biol, 2005. **15**(3): p. 172–8.
42. Yuan, L., et al., *delta-Catenin Regulates Spine Architecture via Cadherin and PDZ-dependent Interactions.* J Biol Chem, 2015. **290**(17): p. 10947–57.
43. Matter, C., et al., *Delta-catenin is required for the maintenance of neural structure and function in mature cortex in vivo.* Neuron, 2009. **64**(3): p. 320–7.
44. Israely, I., et al., *Deletion of the neuron-specific protein delta-catenin leads to severe cognitive and synaptic dysfunction.* Curr Biol, 2004. **14**(18): p. 1657–63.
45. Ramanathan, S., et al., *A case of autism with an interstitial deletion on 4q leading to hemizygosity for genes encoding for glutamine and glycine neurotransmitter receptor*

sub-units (AMPA 2, GLRA3, GLRB) and neuropeptide receptors NPY1R, NPY5R. BMC Med Genet, 2004. **5**: p. 10.
46. El-Amraoui, A. and C. Petit, *Cadherins as targets for genetic diseases.* Cold Spring Harb Perspect Biol, 2010. **2**(1): p. a003095.
47. Mejias, R., et al., *Gain-of-function glutamate receptor interacting protein 1 variants alter GluA2 recycling and surface distribution in patients with autism.* Proc Natl Acad Sci U S A, 2011. **108**(12): p. 4920–5.
48. Bareiss, S., K. Kim, and Q. Lu, *Delta-catenin/NPRAP: A new member of the glycogen synthase kinase-3beta signaling complex that promotes beta-catenin turnover in neurons.* J Neurosci Res, 2010. **88**(11): p. 2350–63.
49. Oh, M., et al., *GSK-3 phosphorylates delta-catenin and negatively regulates its stability via ubiquitination/proteosome-mediated proteolysis.* J Biol Chem, 2009. **284**(42): p. 28579–89.
50. Xue, Y., et al., *GPS 2.0, a tool to predict kinase-specific phosphorylation sites in hierarchy.* Mol Cell Proteomics, 2008. **7**(9): p. 1598–608.
51. Mendez-Vazquez, H., et al., *The autism-associated loss of delta-catenin functions disrupts social behavior.* Proc Natl Acad Sci U S A, 2023. **120**(22): p. e2300773120.
52. Beauchamp, G.K. and K. Yamazaki, *Chemical signalling in mice.* Biochem Soc Trans, 2003. **31**(Pt 1): p. 147–51.
53. Yang, M. and J.N. Crawley, *Simple behavioral assessment of mouse olfaction.* Curr Protoc Neurosci, 2009. **Chapter 8**: p. Unit 8 24.
54. Beery, A.K. and D. Kaufer, *Stress, social behavior, and resilience: insights from rodents.* Neurobiol Stress, 2015. **1**: p. 116–127.
55. Yang, M., J.L. Silverman, and J.N. Crawley, *Automated three-chambered social approach task for mice.* Curr Protoc Neurosci, 2011. **Chapter 8**: p. Unit 8 26.
56. Guang, S., et al., *Synaptopathology Involved in Autism Spectrum Disorder.* Front Cell Neurosci, 2018. **12**: p. 470.
57. Gilbert, J. and H.Y. Man, *Fundamental Elements in Autism: From Neurogenesis and Neurite Growth to Synaptic Plasticity.* Front Cell Neurosci, 2017. **11**: p. 359.
58. Won, H., W. Mah, and E. Kim, *Autism spectrum disorder causes, mechanisms, and treatments: focus on neuronal synapses.* Front Mol Neurosci, 2013. **6**: p. 19.
59. Diering, G.H. and R.L. Huganir, *The AMPA Receptor Code of Synaptic Plasticity.* Neuron, 2018. **100**(2): p. 314–329.
60. Isaac, J.T., M.C. Ashby, and C.J. McBain, *The role of the GluR2 subunit in AMPA receptor function and synaptic plasticity.* Neuron, 2007. **54**(6): p. 859–71.
61. Geiger, J.R., et al., *Relative abundance of subunit mRNAs determines gating and Ca2+ permeability of AMPA receptors in principal neurons and interneurons in rat CNS.* Neuron, 1995. **15**(1): p. 193–204.
62. Rudy, B., et al., *Three groups of interneurons account for nearly 100% of neocortical GABAergic neurons.* Dev Neurobiol, 2011. **71**(1): p. 45–61.
63. Kooijmans, R.N., et al., *Inhibitory interneuron classes express complementary AMPA-receptor patterns in macaque primary visual cortex.* J Neurosci, 2014. **34**(18): p. 6303–15.
64. Adotevi, N.K. and B. Leitch, *Synaptic Changes in AMPA Receptor Subunit Expression in Cortical Parvalbumin Interneurons in the Stargazer Model of Absence Epilepsy.* Front Mol Neurosci, 2017. **10**: p. 434.
65. Kondo, M., R. Sumino, and H. Okado, *Combinations of AMPA receptor subunit expression in individual cortical neurons correlate with expression of specific calcium-binding proteins.* J Neurosci, 1997. **17**(5): p. 1570–81.
66. Pal, B., *Involvement of extrasynaptic glutamate in physiological and pathophysiological changes of neuronal excitability.* Cell Mol Life Sci, 2018. **75**(16): p. 2917–2949.

67. He, K., et al., *Stabilization of Ca2+-permeable AMPA receptors at perisynaptic sites by GluR1-S845 phosphorylation.* Proc Natl Acad Sci U S A, 2009. **106**(47): p. 20033–8.
68. Sanderson, J.L., et al., *AKAP150-anchored calcineurin regulates synaptic plasticity by limiting synaptic incorporation of Ca2+-permeable AMPA receptors.* J Neurosci, 2012. **32**(43): p. 15036–52.
69. Marek, R., et al., *Hippocampus-driven feed-forward inhibition of the prefrontal cortex mediates relapse of extinguished fear.* Nat Neurosci, 2018. **21**(3): p. 384–392.
70. McGarry, L.M. and A.G. Carter, *Inhibitory Gating of Basolateral Amygdala Inputs to the Prefrontal Cortex.* J Neurosci, 2016. **36**(36): p. 9391–406.
71. Delevich, K., et al., *The mediodorsal thalamus drives feedforward inhibition in the anterior cingulate cortex via parvalbumin interneurons.* J Neurosci, 2015. **35**(14): p. 5743–53.
72. Accordino, R.E., et al., *Psychopharmacological interventions in autism spectrum disorder.* Expert Opin Pharmacother, 2016. **17**(7): p. 937–52.
73. Hampson, D.R., S. Gholizadeh, and L.K. Pacey, *Pathways to drug development for autism spectrum disorders.* Clin Pharmacol Ther, 2012. **91**(2): p. 189–200.
74. Min, W.W., et al., *Elevated glycogen synthase kinase-3 activity in Fragile X mice: key metabolic regulator with evidence for treatment potential.* Neuropharmacology, 2009. **56**(2): p. 463–72.
75. Yuskaitis, C.J., et al., *Lithium ameliorates altered glycogen synthase kinase-3 and behavior in a mouse model of fragile X syndrome.* Biochem Pharmacol, 2010. **79**(4): p. 632–46.
76. McManus, E.J., et al., *Role that phosphorylation of GSK3 plays in insulin and Wnt signalling defined by knockin analysis.* EMBO J, 2005. **24**(8): p. 1571–83.
77. Mines, M.A., et al., *GSK3 influences social preference and anxiety-related behaviors during social interaction in a mouse model of fragile X syndrome and autism.* PLoS One, 2010. **5**(3): p. e9706.
78. Kwon, C.H., et al., *Pten regulates neuronal arborization and social interaction in mice.* Neuron, 2006. **50**(3): p. 377–88.
79. Mao, Y., et al., *Disrupted in schizophrenia 1 regulates neuronal progenitor proliferation via modulation of GSK3beta/beta-catenin signaling.* Cell, 2009. **136**(6): p. 1017–31.
80. Kim, W.Y. and W.D. Snider, *Functions of GSK-3 Signaling in Development of the Nervous System.* Front Mol Neurosci, 2011. **4**: p. 44.
81. Wu, X., et al., *Lithium ameliorates autistic-like behaviors induced by neonatal isolation in rats.* Front Behav Neurosci, 2014. **8**: p. 234.
82. Zhang, F., et al., *Inhibitory phosphorylation of glycogen synthase kinase-3 (GSK-3) in response to lithium. Evidence for autoregulation of GSK-3.* J Biol Chem, 2003. **278**(35): p. 33067–77.
83. Ryves, W.J. and A.J. Harwood, *Lithium inhibits glycogen synthase kinase-3 by competition for magnesium.* Biochem Biophys Res Commun, 2001. **280**(3): p. 720–5.
84. O'Brien, W.T. and P.S. Klein, *Validating GSK3 as an in vivo target of lithium action.* Biochem Soc Trans, 2009. **37**(Pt 5): p. 1133–8.
85. Chuang, D.M. and H.K. Manji, *In search of the Holy Grail for the treatment of neurodegenerative disorders: has a simple cation been overlooked?* Biol Psychiatry, 2007. **62**(1): p. 4–6.
86. O'Leary, O. and Y. Nolan, *Glycogen synthase kinase-3 as a therapeutic target for cognitive dysfunction in neuropsychiatric disorders.* CNS Drugs, 2015. **29**(1): p. 1–15.
87. Xu, C., N.G. Kim, and B.M. Gumbiner, *Regulation of protein stability by GSK3 mediated phosphorylation.* Cell Cycle, 2009. **8**(24): p. 4032–9.

88. Siegel, M., et al., *Preliminary investigation of lithium for mood disorder symptoms in children and adolescents with autism spectrum disorder.* J Child Adolesc Psychopharmacol, 2014. **24**(7): p. 399–402.
89. Chokhawala, K., S. Lee, and A. Saadabadi, *Lithium*, in *StatPearls*. 2025: Treasure Island (FL).
90. Baio, J., et al., *Prevalence of Autism Spectrum Disorder Among Children Aged 8 Years - Autism and Developmental Disabilities Monitoring Network, 11 Sites, United States, 2014.* MMWR Surveill Summ, 2018. **67**(6): p. 1–23.
91. Fauzan, N. and N.H. Amran, *Brain Waves and Connectivity of Autism Spectrum Disorders.* Procedia - Social and Behavioral Sciences, 2015. **171**: p. 882–890.
92. Wang, C.G., et al., *Imbalanced Gamma-band Functional Brain Networks of Autism Spectrum Disorders.* Neuroscience, 2022. **498**: p. 19–30.
93. Raj, G.V., et al., *Estrogen receptor coregulator binding modulators (ERXs) effectively target estrogen receptor positive human breast cancers.* Elife, 2017. **6**.
94. Avila, J.A., et al., *Estradiol rapidly increases GluA2-mushroom spines and decreases GluA2-filopodia spines in hippocampus CA1.* Hippocampus, 2017. **27**(12): p. 1224–1229.
95. Wei, J., et al., *Estrogen protects against the detrimental effects of repeated stress on glutamatergic transmission and cognition.* Mol Psychiatry, 2014. **19**(5): p. 588–98.
96. Choleris, E., et al., *Sex differences in the brain: Implications for behavioral and biomedical research.* Neurosci Biobehav Rev, 2018. **85**: p. 126–145.
97. Harms, D.W., et al., *Mouse Genome Editing Using the CRISPR/Cas System.* Curr Protoc Hum Genet, 2014. **83**: p. 15 7 1–27.
98. Kim, S. and E.B. Ziff, *Calcineurin mediates synaptic scaling via synaptic trafficking of Ca2+-permeable AMPA receptors.* PLoS Biol, 2014. **12**(7): p. e1001900.
99. Sztukowski, K., et al., *HIV induces synaptic hyperexcitation via cGMP-dependent protein kinase II activation in the FIV infection model.* PLoS Biol, 2018. **16**(7): p. e2005315.
100. Zaytseva, A., et al., *Ketamine's rapid antidepressant effects are mediated by Ca²⁺-permeable AMPA receptors in the hippocampus.* bioRxiv, 2022: p. 2022.12.05.519102.
101. Kim, J.Y., et al., *Viral transduction of the neonatal brain delivers controllable genetic mosaicism for visualising and manipulating neuronal circuits in vivo.* Eur J Neurosci, 2013. **37**(8): p. 1203–20.
102. Dana, H., et al., *High-performance calcium sensors for imaging activity in neuronal populations and microcompartments.* Nat Methods, 2019. **16**(7): p. 649–657.
103. Dimidschstein, J., et al., *A viral strategy for targeting and manipulating interneurons across vertebrate species.* Nat Neurosci, 2016. **19**(12): p. 1743–1749.
104. Zaytseva, A., et al., *Ketamine's rapid antidepressant effects are mediated by Ca²⁺-permeable AMPA receptors in the hippocampus.* bioRxiv, 2023: p. 2022.12.05.519102.
105. Gleichmann, M. and M.P. Mattson, *Neuronal calcium homeostasis and dysregulation.* Antioxid Redox Signal, 2011. **14**(7): p. 1261–73.
106. Roberts, J.P., et al., *Selective co-activation of alpha7- and alpha4beta2-nicotinic acetylcholine receptors reverses beta-amyloid-induced synaptic dysfunction.* J Biol Chem, 2021: p. 100402.
107. Sun, J.L., et al., *Co-activation of selective nicotinic acetylcholine receptors is required to reverse beta amyloid-induced Ca(2+) hyperexcitation.* Neurobiol Aging, 2019. **84**: p. 166–177.
108. Benson, D.L. and P.A. Cohen, *Activity-independent segregation of excitatory and inhibitory synaptic terminals in cultured hippocampal neurons.* J Neurosci, 1996. **16**(20): p. 6424–32.

109. Kim, S., et al., *Network compensation of cyclic GMP-dependent protein kinase II knockout in the hippocampus by Ca2+-permeable AMPA receptors.* Proc Natl Acad Sci U S A, 2015. **112**(10): p. 3122–7.
110. Kim, S., C.J. Violette, and E.B. Ziff, *Reduction of increased calcineurin activity rescues impaired homeostatic synaptic plasticity in presenilin 1 M146V mutant.* Neurobiol Aging, 2015. **36**(12): p. 3239–46.
111. Shou, J., et al., *Distinct Roles of GluA2-lacking AMPA Receptor Expression in Dopamine D1 or D2 Receptor Neurons in Animal Behavior.* Neuroscience, 2019. **398**: p. 102–112.
112. Phillips, M.L., H.A. Robinson, and L. Pozzo-Miller, *Ventral hippocampal projections to the medial prefrontal cortex regulate social memory.* Elife, 2019. **8**.
113. Kim, S., et al., *Brain region-specific effects of cGMP-dependent kinase II knockout on AMPA receptor trafficking and animal behavior.* Learn Mem, 2016. **23**(8): p. 435–41.
114. Lee, R., et al., *Co-activation of selective nicotinic acetylcholine receptor subtypes is required to reverse hippocampal network dysfunction, fear memory loss, and amyloid pathology in Alzheimer's disease.* bioRxiv, 2025.